

CONTROL OF NEURAL FIELD EQUATIONS WITH STEP-FUNCTION INPUTS*

CYPRIEN TAMEKUE[†] AND SHINUNG CHING[†]

Abstract. Wilson-Cowan and Amari-type models capture nonlinear neural population dynamics, providing a fundamental framework for modeling how sensory and other exogenous inputs shape activity in neural tissue. We study the controllability properties of Amari-type neural fields subject to piecewise/constant-in-time inputs. The model describes the time evolution of the polarization of neural tissue within a spatial continuum, with synaptic interactions represented by a convolution kernel. We study the synthesis of piecewise/constant-in-time inputs to achieve two-point boundary-type control objectives, namely, steering neural activity from an initial state to a prescribed target state. This approach is particularly relevant for predicting the emergence of paradoxical neural representations, such as discordant visual illusions that occur in response to overt sensory stimuli. We first present a control synthesis based on the Banach fixed-point theorem, which yields an iterative construction of a constant-in-time input under minimal regularity assumptions on the kernel and transfer function; however, it exhibits practical limitations, even in the linear case. To overcome these challenges, we then develop a generic synthesis framework based on the flow of neural dynamics drift, enabling explicit piecewise constant and constant-in-time inputs. Extensive numerical results in one and two spatial dimensions confirm the effectiveness of the proposed syntheses and demonstrate their superior performance compared to inputs derived from naive linearization at the initial or target states when these states are not equilibria of the drift dynamics. By providing a mathematically rigorous framework for controlling Amari-type neural fields, this work advances our understanding of nonlinear neural population control with potential applications in computational neuroscience, psychophysics, and neurostimulation.

Key words. Nonlinear control, control synthesis, step controllability, neural field equations, spatially forced pattern forming system, predicting visual illusions.

MSC codes. 93C20, 92C20, 93C10, 35Q92, 93B50.

1. Introduction. Wilson-Cowan [55] and Amari-type [2] equations are neural field models that describe the nonlinear dynamics of interacting populations of excitatory and inhibitory neurons at the scale of a cortical macrocolumn (a roughly 1mm diameter section of the cortex). These models are favored for their balance of biophysical interpretability and mathematical tractability. They have been instrumental in exploring a range of questions in theoretical neuroscience, such as how sensory inputs drive neural activity, particularly in visual perception contexts [6, 10, 12, 24, 39, 42, 49, 50, 51]. For example, the steady-state solutions of Amari-type equations have been used to mechanistically model visual illusions, such as the visual MacKay effect or Billock and Tsou experiments [10, 49, 50, 51], as asymptotic outcomes of cortical activity driven by sensory inputs.

An important emerging question in the analysis of neural field models pertains to their controllability properties [50], i.e., the extent to which they are labile with respect to exogenous inputs. Such analysis provides a mathematical foundation for both scientific and engineering focus. For instance, the determination of how sensory inputs drive the formation of neural representations or how external stimulation of the brain may modify brain dynamics in clinical contexts. This perspective advances the theoretical understanding of neural dynamics and opens new avenues for practical applications, such as predicting or designing visual stimuli that induce targeted perceptual effects.

In this paper, we study control analysis and synthesis for neural field equations of the Amari-type with sensory inputs that are constant in time. The considered equation reads as

$$(NF) \quad \begin{aligned} \partial_t a(x, t) + \alpha a(x, t) - \mu \int_{\mathbb{R}^d} \omega(x, y) f(a(y, t)) dy &= I(x), & (t, x) \in \mathbb{R}_+ \times \mathbb{R}^d \\ a(x, 0) &= a_0(x), & x \in \mathbb{R}^d. \end{aligned}$$

Here, $d \in \mathbb{N}^*$ (but it is usually taken to be one or two) where \mathbb{N}^* stands for the set of positive integers, and $\mathbb{R}_+ := [0, \infty)$. The time-evolution of the average membrane potential at time $t \geq 0$ is given by the map

*

Funding: This work is partially supported by grant R21MH132240 from the US National Institutes of Health to SC.

[†]Department of Electrical and Systems Engineering, Washington University in St. Louis, St. Louis, 63130, MO, USA. (cyprien@wustl.edu, shinung@wustl.edu).

$x \mapsto a(x, t)$, and the state of cortical activity at time $t = 0$ is assumed to be provided by the function a_0 . Here, $\alpha > 0$ is the time scale of activity decay, I is a constant in time input, and the transfer function f captures the nonlinear response of neurons after activation. At the same time, the parameter $\mu > 0$ measures the strength of neuronal interaction. Finally, the kernel $\omega(x, y) = \omega(x - y)$ models the synaptic connections between neurons at two different locations x and y . We refer to [17, 19] for a recent overview of neural population models.

Although (NF) is one of the most parsimonious neural population models widely used to mechanistically describe diverse neurological and visual phenomena (see, e.g., [11, 23] for reviews), it inherently neglects the finite time required for stimulus—represented by the input I —to propagate between neurons at different cortical locations. Specifically, (NF) assumes infinite axonal transmission speed between a presynaptic neuron at y and a postsynaptic neuron at x . In practice, conduction velocities vary across neural populations and typically range from about 1 m/s to 100 m/s [46]. Incorporating such finite transmission delays gives rise to delayed neural field equations, which have been extensively studied both theoretically and numerically; see, for instance, [15, 21, 26, 45, 53]. Notably, transmission delays play a crucial role in the emergence of oscillatory dynamics linked to neurological disorders such as Parkinson’s disease [4, 40].

In this work, we deliberately focus on the delay-free formulation (NF) for two main reasons. First, despite its simplicity, it still captures a wide range of neural processes. Second, establishing a control framework in this setting provides a robust foundation for addressing more complex models that include state-dependent delays.

It is also worth noting that a more realistic model would treat cortical tissue as a bounded domain $\Omega \subset \mathbb{R}^d$ rather than the entire space \mathbb{R}^d ; see, for example, [54, Section 7.1]. To mitigate this idealization, we assume that the connectivity kernel ω decays rapidly at infinity, resembling a “Mexican hat” or “wizard hat” shape.

Finally, because our control synthesis is formulated in terms of the flow maps generated by the neural field dynamics, the results naturally extend to inhomogeneous kernels (i.e., $\omega(x, y) \neq \omega(x - y)$) or bounded domains Ω , provided suitable assumptions on ω ensure the applicability of the synthesis framework.

To the authors’ knowledge, the controllability and stability properties of neural field equations like (NF) have been considered for absolute stability of homogeneous solutions [25], for feedback stabilization of deep-brain stimulation [14, 15] (see also [3, 13] for observability properties of these equations) or for open-loop control of traveling waves [56]. We also refer to [20, p. 28] for a related *full-field inverse neural problem*, where the authors investigated how to construct the kernel ω under the assumption that both the initial state $a_0(x)$ and the solution $a(x, t)$ are known for all x and t . A general controllability question—the ability to steer the system from an initial state to a given target state—was engaged in [50]. The latter work has provided new insights into the ability of a constant in time input to steer the solution of (NF) from an initial state to a desired target state in a small time horizon. While [50] proposes synthesizing such inputs, the implicit dependence on an abstract operator, denoted $\mathcal{O}(\tau)$, poses challenges for practical application, particularly as $\mathcal{O}(\tau)$ depends on the state a and the input I even for a small time horizon.

From a neural control standpoint, a feedforward synthesis of a constant in time input that approximately solves the control objective is valuable, especially in modeling visual illusions where transient dynamics may play a critical role. This is particularly relevant for understanding how specific sensory stimuli, modeled as constant in time inputs, influence cortical dynamics in transient regimes. Noninvasive neurostimulation techniques, such as transcranial Direct Current Stimulation (tDCS), can also benefit from constant in time input synthesis for small time horizons. In tDCS, weak constant electrical currents are applied to modulate brain activity [5], and modeling these effects can help predict how sustained stimulation influences neural dynamics over short time intervals [43, Section 11.10]. Such an approach may be relevant for emerging interests in translational neuroscience, such as the use of tDCS for memory enhancement [30] and other therapeutic applications.

The open-loop control synthesis with constant-in-time inputs can also be used to mechanistically steer the neural field equation (NF) toward generating a desired stationary pattern over a short time horizon—even patterns that would not spontaneously emerge under the given parameter regime, such as when $\mu = \mu_c$, $\mu < \mu_c$, or $\mu > \mu_c$ (see (1.5) for the definition of the critical parameter μ_c). In his seminal work [2], Amari analyzed conditions under which spatial patterns of neural activity—such as homogeneous active states, localized bumps, traveling waves, or stripes—can arise in the absence of external input, driven purely by spontaneous symmetry-breaking due to noise or initial heterogeneity.

It is well established that for sufficiently small values of the gain parameter μ , specifically when $\mu < \mu_c$, only the trivial or homogeneous active state exists and is globally exponentially stable. However, when μ exceeds the critical threshold μ_c , localized bump solutions can emerge through a reversible Hopf bifurcation with 1:1 resonance [27]; see also [18, 22]. As a result, in the absence of external input and starting from a homogeneous initial state a_0 , the solution to (NF) remains homogeneous for all $T > 0$ if $\mu < \mu_c$. Nevertheless, our numerical illustrations (in both one- and two-dimensional spatial domains) show that the proposed generic constant-in-time input syntheses can robustly drive the system from a homogeneous state to a localized bump state within an arbitrarily small time horizon, even in parameter regimes where such patterns would not arise spontaneously.

The remainder of the paper is organized as follows. Section 1.1 introduces the general notations used throughout the paper, together with the assumptions considered in the parameters in (NF). In Section 2.1, we begin by directly integrating (NF) to derive an implicit control synthesis based on the Banach fixed-point theorem, and we highlight its limitations even in the linear setting. To overcome these drawbacks, Section 2.2 presents the generic synthesis results of the paper. Section 2.2.1 reformulates (NF) in an abstract form, setting the stage for a more general control framework. Section 2.2.2 addresses the well-posedness of the dynamics by giving a solution representation that underpins the proposed synthesis, while Section 3 discusses the practical feasibility of the proposed generic synthesis inputs. Section 4 provides remarks and outlines directions for further investigation. In Section 5, we discuss how the developed constant-in-time input syntheses can be leveraged to predict or induce visual illusions in a mechanistic modeling context. Numerical illustrations supporting the effectiveness of the proposed control inputs are reported in Section 6. The main proofs are collected in Section A, and technical auxiliary results are deferred to Appendix B.

Notation 1.1. Unless otherwise stated, p will denote a real number satisfying $1 \leq p \leq \infty$, and q will denote the conjugate to p given by $1/p + 1/q = 1$. We adopt the convention that the conjugate of $p = 1$ is $q = \infty$ and vice-versa. For $d \in \mathbb{N}^*$, we denote by $L^p(\mathbb{R}^d)$ the Lebesgue space of class of real-valued measurable functions u on \mathbb{R}^d such that $|u|$ is integrable over \mathbb{R}^d if $p < \infty$, and $|u|$ is essentially bounded over \mathbb{R}^d when $p = \infty$. We endow these spaces with their standard norms

$$\|u\|_p^p = \int_{\mathbb{R}^d} |u(x)|^p dx \quad \text{and} \quad \|u\|_\infty = \operatorname{ess\,sup}_{x \in \mathbb{R}^d} |u(x)|.$$

We use $\mathcal{L}(X, Y)$ to denote the space of linear bounded operators between two normed vector spaces X and Y , and simply $\mathcal{L}(X)$ when $X = Y$. If $A \in \mathcal{L}(X)$, then $e^A \in \mathcal{L}(X)$ and $\sigma(A)$ are, respectively, the exponential operator and the spectrum of the operator A defined by

$$(1.1) \quad e^A = \sum_{n=0}^{\infty} \frac{A^n}{n!} \quad \text{and} \quad \sigma(A) = \mathbb{C} \setminus \rho(A)$$

where $\rho(A) := \{\lambda \in \mathbb{C} \mid A - \lambda \operatorname{Id} \in \mathcal{L}(X) \text{ is one to one and onto}\}$.

For $x \in \mathbb{R}^d$, we denote by $|x|$ its Euclidean norm, and the scalar product with $\xi \in \mathbb{R}^d$ is defined by $\langle x, \xi \rangle = x_1 \xi_1 + x_2 \xi_2 + \dots + x_d \xi_d$. Let $\mathcal{S}(\mathbb{R}^d)$ be the Schwartz space of rapidly-decreasing $C^\infty(\mathbb{R}^d)$ functions. The Fourier transform of $u \in \mathcal{S}(\mathbb{R}^d)$ is defined by

$$(1.2) \quad \widehat{u}(\xi) := \mathcal{F}\{u\}(\xi) = \int_{\mathbb{R}^d} u(x) e^{-2\pi i \langle x, \xi \rangle} dx \quad \forall \xi \in \mathbb{R}^d.$$

The spatial convolution of two functions $u \in L^1(\mathbb{R}^d)$ and $v \in L^p(\mathbb{R}^d)$, $1 \leq p \leq \infty$ is defined by

$$(1.3) \quad (u * v)(x) = \int_{\mathbb{R}^d} u(x-y)v(y) dy \quad \forall x \in \mathbb{R}^d.$$

Finally, we recall that for every $w \in L^p(\mathbb{R}^d)$, $1 \leq p < \infty$, its dual $w^* := w|w|^{p-2} \|w\|_p^{2-p} \in L^q(\mathbb{R}^d)$. Moreover, for $1 < p < \infty$, the mapping $\varphi : L^p(\mathbb{R}^d) \rightarrow \mathbb{R}$, $w \mapsto \varphi(w) = \|w\|_p^2/2$ is differentiable and $D\varphi(w)\phi = \langle w^*, \phi \rangle_{L^q, L^p}$,

for all $w, \phi \in L^p(\mathbb{R}^d)$ where

$$(1.4) \quad \langle w^*, \phi \rangle_{L^q, L^p} := \int_{\mathbb{R}^d} w^*(x) \phi(x) dx.$$

For $p = 2$, it coincides with the usual scalar product in $L^2(\mathbb{R}^d)$ that we denote as $\langle w^*, \phi \rangle_{L^2} = \langle w, \phi \rangle_{L^2}$.

Assumptions 1.2. Unless otherwise stated, we assume that the transfer function f belongs to the class $C^2(\mathbb{R})$, is non-decreasing, f' , and f'' are bounded so that f and f' are globally Lipschitz on \mathbb{R} . For clarity in the presentation, one assumes that $f(0) = 0$ and $\|f'\|_\infty = 1$. The later are without loss of generality since we can replace¹ f by $\tilde{f}(s) = f(\lambda s) - f(0)$ with $\lambda := 1/\|f'\|_\infty$.

We also assume² that the connectivity kernel $\omega \in \mathcal{S}(\mathbb{R}^d)$, and we introduce the parameters

$$(1.5) \quad \mu_0 := \frac{\alpha}{\|\omega\|_1} \quad \mu_1 := \frac{\alpha}{\|\widehat{\omega}\|_\infty}, \quad \mu_c := \frac{\alpha}{\|\widehat{\omega}\|_\infty f'(0)}.$$

that we will refer to when needed. Then, $\mu_0 \leq \mu_1 \leq \mu_c$, the parameter μ_0 (μ_1 if $p = 2$) appears as the natural largest value of μ up to which (NF) admits a unique stationary state which is globally exponentially stable in the space $L^p(\mathbb{R}^d)$ (see, for instance, [48]), and when $d = 2$, assuming $\mu < \mu_0$ ($\mu < \mu_1$ if $p = 2$) enables the modeling of certain visual illusions [10, 49, 50, 51] using (NF). Whereas the parameter μ_c is referred to as the bifurcation point of the homogeneous state (which correspond to $a = 0$ since it is assumed that $f(0) = 0$) and corresponds to the value of μ where (NF) generates certain geometric hallucinatory patterns [12, 24] that spontaneously emerge in the primary visual cortex (V1 henceforth) or visual illusions [39] when a state-dependent sensory input drives V1' activity. See also [54] for the analysis of persistent states that emerge at this point.

Remark 1.3. Note that we do not explicitly require f to be bounded.

2. Main Results. This section presents the main theoretical contributions of the paper. Section 2.1 introduces a constructive control synthesis based on the Banach fixed-point theorem. Relying on standard assumptions for the transfer function and connectivity kernel, this method yields an iterative scheme for synthesizing constant-in-time inputs that steer the system from a given initial state to a prescribed target.

Although effective under appropriate conditions, this approach—illustrated through the linear case—reveals intrinsic limitations: it fails to fully characterize the controllability properties for constant inputs, especially in critical or supercritical regimes of the parameter μ . These shortcomings motivate the development of a more general and robust synthesis framework in Section 2.2.

Before defining the notion of controllability that we are considering in this paper, let us recall the following definition. See, for instance, [52, Remark 4.2.3].

DEFINITION 2.1. *A step function on $[0, T]$ with values in $L^p(\mathbb{R}^d)$ is a piecewise constant in time function defined on $[0, T]$ with values in $L^p(\mathbb{R}^d)$. Constant in time functions $I \in L^p(\mathbb{R}^d)$ on $[0, T]$ are natural examples of such functions.*

DEFINITION 2.2 (Step controllability). *Let $1 \leq p \leq \infty$ and $T > 0$. We say that (NF) is step controllable over the time interval $[0, T]$ if, for all $(a_0, a_1) \in L^p(\mathbb{R}^d)^2$, there exists a step function I on $[0, T]$ with value in $L^p(\mathbb{R}^d)$ such that the solution of (NF) with $a(0) = a_0$ satisfies $a(T) = a_1$.*

2.1. Synthesis based on the Banach fixed-point theorem. In this section—and only here—we assume that the transfer function f is non-decreasing, globally Lipschitz continuous, and differentiable at 0. We also assume only that the connectivity kernel $\omega \in L^1(\mathbb{R}^d)$. Under these assumptions, the parameters μ_0 , μ_1 , and μ_c remain well-defined as given in (1.5).

Within this setting, we begin with the following well-posedness result, the proof of which can be found in [54] or by invoking classical textbooks such as [41, Chapter 6].

¹This change of functions yields (NF) with kernel $\tilde{\omega} = \omega/\lambda$, and input $\tilde{I} = -\mu f(0)\tilde{\omega}(0) + I/\lambda$.

²If one works in $L^p(\mathbb{R}^d)$ for a particular $1 \leq p \leq \infty$, it is sufficient that $\omega \in L^1(\mathbb{R}^d) \cap L^p(\mathbb{R}^d) \cap L^q(\mathbb{R}^d)$. Indeed, $\omega \in L^1(\mathbb{R}^d) \cap L^p(\mathbb{R}^d)$ as highlighted in [50, Remark 4.5], and $\omega \in L^q(\mathbb{R}^d)$ as it is required for some of our main results in this paper.

PROPOSITION 2.3. *Let $p \in [1, \infty]$ and $(a_0, I) \in L^p(\mathbb{R}^d) \times L^\infty([0, \infty); L^p(\mathbb{R}^d))$. There exists a unique solution $a_I \in C^0([0, \infty); L^p(\mathbb{R}^d))$ to (NF). Letting $a_I(t) := a_I(\cdot, t)$, one has the following representation*

$$(2.1) \quad a_I(t) = e^{-\alpha t} a_0 + \mu \int_0^t e^{-\alpha(t-s)} \omega * f(a_I(s)) ds + \int_0^t e^{-\alpha(t-s)} I(s) ds, \quad \forall t \geq 0.$$

Moreover, the following estimate holds

$$(2.2) \quad \|a_I(t)\|_p \leq e^{-\alpha t(1-\frac{\mu}{\mu_0})} \|a_0\|_p + t \max(1, e^{-\alpha t(1-\frac{\mu}{\mu_0})}) \sup_{0 \leq \tau \leq t} \|I(\tau)\|_p, \quad \forall t \geq 0.$$

As is common in control synthesis approaches, determining a constant-in-time input that steers the system (NF) from an initial state a_0 to a target state $a_1 \in L^p(\mathbb{R}^d)$ over a finite time horizon $T > 0$ amounts to solving, for $I \in L^p(\mathbb{R}^d)$, the terminal condition $a_I(T) = a_1$, where $a_I(\cdot)$ denotes the solution of (NF) associated with the input I . Substituting into the implicit solution representation (2.1), the requirement $a_I(T) = a_1$ yields the condition that $I \in L^p(\mathbb{R}^d)$ must satisfy

$$(2.3) \quad I = \alpha(1 - e^{-\alpha T})^{-1} \left\{ a_1 - e^{-\alpha T} a_0 - \mu \int_0^T e^{-\alpha(T-t)} \omega * f(a_I(t)) dt \right\}.$$

Equation (2.3) is implicit w.r.t. the unknown $I \in L^p(\mathbb{R}^d)$, and the key challenge lies in identifying conditions under which it admits at least one solution that is numerically implementable. This motivates the main result of this section, which relies on the Banach fixed-point theorem. The proof is outlined in Section A.1.

THEOREM 2.4. *Let $p \in [1, \infty]$ and $(a_0, a_1) \in L^p(\mathbb{R}^d)^2$. Define the sequence $(I_n)_n \subset L^p(\mathbb{R}^d)$ by*

$$(2.4) \quad \begin{cases} I_0 \in L^p(\mathbb{R}^d) \\ I_{n+1} = \alpha(1 - e^{-\alpha T})^{-1} \left\{ a_1 - e^{-\alpha T} a_0 - \mu \int_0^T e^{-\alpha(T-t)} \omega * f(a_{I_n}(t)) dt \right\}, & n \geq 0 \\ a_{I_n} \in L^p(\mathbb{R}^d) \text{ solution of } \dot{a}(t) = -\alpha a(t) + \mu \omega * f(a(t)) + I_n, & a(0) = a_0. \end{cases}$$

Assume that one of the following conditions holds

1. $T > 0$ and $\mu < \mu_0/2$;
2. $T < T_*(\frac{\mu}{\mu_0})$ and $\mu \geq \mu_0$ where $T_*(\frac{\mu}{\mu_0}) > 0$ is the unique solution of $L(T) = 1$ with

$$(2.5) \quad L(T) := \begin{cases} \frac{\alpha T}{1 - e^{-\alpha T}} - 1 & \text{if } \mu = \mu_0 \\ \frac{1}{r-1} \left(\frac{e^{\alpha r T} - 1}{e^{\alpha T} - 1} - r \right) & \text{if } r := \mu/\mu_0 \neq 1. \end{cases}$$

Then, $(I_n)_n$ converges in $L^p(\mathbb{R}^d)$ to $I \in L^p(\mathbb{R}^d)$ given by (2.3) and the corresponding solution $a_I(\cdot)$ to (NF) satisfies $a_I(T) = a_1$.

Remark 2.5. In Proposition 2.3 and Theorem 2.4, one can replace μ_0 by μ_1 in the case of $p = 2$ to get sharp results. This is justified via a Fourier transform argument using Parseval's identity and Plancherel's theorem. See, for instance, the proof of Lemma B.3.

Remark 2.6. Theorem 2.4 provides an implementable iterative synthesis of a constant in time input that steers (NF) from a given initial state $a_0 \in L^p(\mathbb{R}^d)$ to any target state $a_1 \in L^p(\mathbb{R}^d)$ over a finite time horizon $T > 0$. However, the result comes with the following limitations

1. It covers the *subcritical regime* $\mu < \mu_0$ for all $T > 0$ if $\mu < \mu_0/2$;
2. It covers the *critical* and the *supercritical regime* $\mu \geq \mu_0$ if $T < T_*(\mu/\mu_0)$, where $T_*(\cdot) > 0$ decreases as μ/μ_0 increases.

We can also highlight the limitations of Theorem 2.4 by comparing it to the linear case, as stated in the following proposition. The proof is straightforward.

PROPOSITION 2.7. *Let $p \in [1, \infty]$, $T > 0$ and $a_0 \in L^p(\mathbb{R}^d)$. Consider the linear dynamics*

$$(2.6) \quad \dot{a}(t) = Aa(t) + I, \quad a(0) = a_0, \quad t \in [0, T]$$

where $Au = -\alpha u + \mu\omega * u$, $u \in L^p(\mathbb{R}^d)$. Assume that the following spectral condition holds

$$(2.7) \quad \sigma(A) \cap \left\{ i \frac{2\pi\ell}{T} \in \mathbb{C} \mid \ell \in \mathbb{Z} \right\} = \emptyset.$$

Then, the solution $a_I \in C^\infty([0, T]; L^p(\mathbb{R}^d))$ of (2.6) satisfies $a_I(T) = a_1 \in L^p(\mathbb{R}^d)$, if and only if, the constant in time input $I \in L^p(\mathbb{R}^d)$ is given by

$$(2.8) \quad I = (e^{TA} - \text{Id})^{-1}A(a_1 - e^{TA}a_0).$$

LEMMA 2.8. *The spectral condition in (2.7) is automatically satisfied if $\mu < \mu_0$, or, in the specific case where $p = 2$, if $\mu < \mu_1$. In particular, under these conditions, $I \in L^p(\mathbb{R}^d)$ in (2.8) is well-defined.*

Proof. Let $t \in \mathbb{R}_+$. One proves as in Lemma B.3 that

$$(2.9) \quad \|e^{tA}\|_{\mathcal{L}(L^p(\mathbb{R}^d))} \begin{cases} \leq e^{-\alpha(1-\frac{\mu}{\mu_0})t} & \text{if } 1 \leq p \leq \infty \\ \leq e^{-\alpha(1-\frac{\mu}{\mu_1})t} & \text{if } p = 2. \end{cases}$$

It follows that $\|e^{tA}\|_{\mathcal{L}(L^p(\mathbb{R}^d))} < 1$ for every $t > 0$ if $\mu < \mu_0$ (or $\mu < \mu_1$ when $p = 2$). The first part of the lemma follows, and the second part then follows from the Neumann series expansion. \square

Proposition 2.7 ensures that in the linear case (i.e., when $f(s) = s$), a constant-in-time input that steers (NF) from an initial state a_0 to a target state a_1 over a finite time horizon $T > 0$ can be constructed explicitly in a feedforward manner. Notably, this input is well-defined only under the spectral condition specified in (2.7), which is less restrictive than those required in Theorem 2.4.

The objective of the next section is to properly generalize this result to the fully nonlinear setting.

2.2. Generic syntheses: Proper generalization of the linear case. This section introduces generic synthesis formulations that extend the linear case in a principled manner. Section 2.2.1 recasts the system (NF) within an abstract functional framework tailored to control-theoretic analysis and synthesis. In contrast to the fixed-point approach of Section 2.1, which requires only mild assumptions on f , this formulation imposes stronger smoothness conditions (see Assumptions 1.2), which are crucial for exploiting the flow maps of the drift dynamics in constructing a general synthesis theory.

2.2.1. Abstract Formulation. For our purpose to extend the linear controllability results presented in Proposition 2.7 in the fully nonlinear case, we recast (NF) as follows

$$(2.10) \quad \dot{a}(t) = N(a(t)) + I, \quad a(0) = a_0$$

where for any $1 \leq p \leq \infty$, the nonlinear map N is given by

$$(2.11) \quad N(u) = -\alpha u + \mu\omega * f(u), \quad u \in L^p(\mathbb{R}^d).$$

Equation (2.10) defines an ordinary differential equation in the Banach space $L^p(\mathbb{R}^d)$ associated with N . Recall from [50, Lemma 3.2] that for every $1 \leq p \leq \infty$, N is (globally) Lipschitz continuous from $L^p(\mathbb{R}^d)$ to itself. Therefore, one can define a (nonlinear) flow of operators $\{U_t \mid t \in \mathbb{R}\}$ in $L^p(\mathbb{R}^d)$ generated by N such that for any $a_0 \in L^p(\mathbb{R}^d)$, $U_t(a_0)$ is the solution to (2.10) when $I \equiv 0$, namely

$$(2.12) \quad \frac{d}{dt}U_t(a_0) = N(U_t(a_0)), \quad U_0(a_0) = a_0.$$

Denote by V_t the inverse of U_t for $t \in \mathbb{R}$, i.e., $V_t(a_0) = U_{-t}(a_0)$ for all $a_0 \in L^p(\mathbb{R}^d)$. Then, it holds

$$(2.13) \quad \frac{d}{dt}V_t(a_0) = -N(V_t(a_0)), \quad V_0(a_0) = a_0.$$

By Assumptions 1.2, it follows, for example, from³ [50, Lemma B.8] that for every $1 < p \leq \infty$, $N \in C^1(L^p(\mathbb{R}^d); L^p(\mathbb{R}^d))$ (Gâteaux differentiable when $p = 1$) and the operator norm of the Fréchet derivative $DN(\psi)$ is uniformly bounded w.r.t. $\psi \in L^p(\mathbb{R}^d)$,

$$(2.14) \quad \|DN(\psi)\|_{\mathcal{L}(L^p(\mathbb{R}^d))} \begin{cases} \leq \alpha + \mu\|\omega\|_1 & \text{if } 1 < p \leq \infty \\ \leq \alpha + \mu\|\widehat{\omega}\|_\infty & \text{if } p = 2 \end{cases} \quad \forall \psi \in L^p(\mathbb{R}^d).$$

Here the differential $DN(\psi) \in \mathcal{L}(L^p(\mathbb{R}^d))$ at every $\psi \in L^p(\mathbb{R}^d)$ is given by (see, [50, Lemma B.8])

$$(2.15) \quad DN(\psi)\phi = -\alpha\phi + \mu\omega * [f'(\psi)\phi] \quad \forall \phi \in L^p(\mathbb{R}^d).$$

In particular, for any fixed $t \in \mathbb{R}$, U_t and V_t are Fréchet differentiable for every $a_0 \in L^p(\mathbb{R}^d)$. If we use $DU_t(a_0)$ and $DV_t(a_0)$ to denote, respectively, the evaluation of these Fréchet derivatives at any $a_0 \in L^p(\mathbb{R}^d)$, then they solve, respectively, the following

$$(2.16) \quad \begin{cases} \frac{d}{dt}DU_t(a_0) & = DN(U_t(a_0))DU_t(a_0) \\ DU_0(a_0) & = \text{Id}, \end{cases} \quad \begin{cases} \frac{d}{dt}DV_t(a_0) & = -DN(V_t(a_0))DV_t(a_0) \\ DV_0(a_0) & = \text{Id}. \end{cases}$$

Moreover, it follows from⁴ [50, Lemma B.10] that $DU_t(a_0)$ is a well-defined invertible operator, and

$$(2.17) \quad [DU_t(a_0)]^{-1} = DV_t(U_t(a_0)), \quad t \in \mathbb{R}, a_0 \in L^p(\mathbb{R}^d).$$

2.2.2. Representations and series expansions of the solution. This section provides dual representations of the solution to (NF) and its series expansions based on the abstract formulation of Section 2.2.1. These representations emerge from the chronological calculus-inspired framework introduced by Agrachev and Gamkrelidze in the late 1970s [1] to represent the solutions of nonautonomous ordinary differential equations on finite-dimensional manifolds.

To the best of the authors' knowledge, this representation framework was first used in [50] in the context of (NF) and later instantiated in finite-dimensional settings in [47] to enable synthesis in continuous-time Hopfield-type recurrent neural networks with underactuated constant inputs.

For completeness, we present these representations in the general case of time-varying inputs. We start with the first solution representation that can be viewed as a natural extension of the solution representation in the linear case (Duhamel's formula [41, p. 105]), particularly at the final time horizon T , with the nonlinear flow and its differential replacing the exponential operator. In particular, it can be termed as a backward representation of the solution to (2.10). The proof of the following is given in Section A.2.

THEOREM 2.9. *Let $p \in (1, \infty]$ and $T > 0$. For all $(a_0, I) \in L^p(\mathbb{R}^d) \times L^1((0, T); L^p(\mathbb{R}^d))$, the solution $a \in C^0([0, T]; L^p(\mathbb{R}^d))$ to (2.10) can be expressed as*

$$(2.18) \quad a(t) = U_{t-T} \left(U_T(a_0) + \int_0^t DU_{T-s}(a(s))I(s) ds \right), \quad \forall t \in [0, T].$$

The second solution representation, termed as a forward representation of the solution to (2.10), is as follows. The proof is identical to that of Theorem 2.9.

³For a detailed discussion of the notions of Fréchet and Gâteaux derivatives, see, for example, [16, Chapter 7].

⁴The result in [50, Lemma B.10] proved the invertibility of $DU_t(a_0)$ for every $t \geq 0$. However, this can be straightforwardly extended to $t \in \mathbb{R}$ since U_t is well-defined for all $t \in \mathbb{R}$.

THEOREM 2.10. *Let $p \in (1, \infty]$ and $T > 0$. For all $(a_0, I) \in L^p(\mathbb{R}^d) \times L^1((0, T); L^p(\mathbb{R}^d))$, the solution $a \in C^0([0, T]; L^p(\mathbb{R}^d))$ to (2.10) can be expressed as*

$$(2.19) \quad a(t) = U_t \left(a_0 + \int_0^t DV_s(a(s))I(s)ds \right), \quad \forall t \in [0, T].$$

Remark 2.11. Theorems 2.9 and 2.10 are stated for $p \in (1, \infty]$, thereby excluding the case $p = 1$. This restriction stems from the fact that the (Fréchet) derivative operators $DU_t(a_0)$ and $DV_t(a_0)$, defined for $a_0 \in L^p(\mathbb{R}^d)$, are well-defined only when $p \in (1, \infty]$. This follows from [50, Lemma B.8], which establishes that the nonlinear map N is Fréchet differentiable only in this range of p .

Whether N is Fréchet differentiable in $L^1(\mathbb{R}^d)$ remains unclear. The proof of Fréchet differentiability in [50, Lemma B.8] relies on a classical result (see, e.g., [38, Proposition 2.8, p. 60]): let \mathcal{X} and \mathcal{Y} be normed vector spaces, and let $g : \mathcal{X} \rightarrow \mathcal{Y}$. If g is Gâteaux differentiable and its Gâteaux derivative $\partial g : \mathcal{X} \rightarrow \mathcal{L}(\mathcal{X}, \mathcal{Y})$ is continuous, then g is Fréchet differentiable and belongs to $C^1(\mathcal{X}, \mathcal{Y})$.

In [50, Lemma B.8], the authors showed that the Gâteaux derivative of N is not continuous from $L^1(\mathbb{R}^d)$ to $\mathcal{L}(L^1(\mathbb{R}^d))$. While this does not rule out Fréchet differentiability in $L^1(\mathbb{R}^d)$, it implies that if N were Fréchet differentiable in $L^1(\mathbb{R}^d)$, the map $DN : L^1(\mathbb{R}^d) \rightarrow \mathcal{L}(L^1(\mathbb{R}^d))$ could not be continuous. In other words, N could not belong to $C^1(L^1(\mathbb{R}^d); L^1(\mathbb{R}^d))$.

Building on the solution representation in Theorem 2.9, the following proposition outlines the expansion strategy that forms the foundation of our subsequent analysis and inputs synthesis. The proof is provided in Section A.3.

PROPOSITION 2.12. *Let $p \in [2, \infty]$, $\tau > 0$ and $T \geq \tau$. Let $a_0 \in L^p(\mathbb{R}^d)$, and $I_{sf, \tau} \in L^1((0, T); L^p(\mathbb{R}^d))$ be the step function defined by*

$$(2.20) \quad I_{sf, \tau}(t) = \begin{cases} 0 & \text{if } 0 \leq t \leq T - \tau \\ I & \text{if } T - \tau < t \leq T \end{cases}$$

where $I \in L^p(\mathbb{R}^d)$. Then, the solution $a_\tau(\cdot)$ to (2.10) corresponding to $I_{sf, \tau}$ expands at time $t = T$ as

$$(F1) \quad a_\tau(T) = U_T(a_0) - \sum_{n=0}^{\infty} \frac{(-\tau)^{n+1} DN(U_T(a_0))^n}{(n+1)!} DU_\tau(U_{T-\tau}(a_0))I - \varphi_{\tau, T}(I)I.$$

Here $\varphi_{\tau, T}(I) := \kappa_{\tau, T}(I) + \chi_{\tau, T}(I)$ with

$$(2.21) \quad \kappa_{\tau, T}(I) = \sum_{n=1}^{\infty} \int_0^\tau \frac{(-1)^n t^{n+1}}{(n+1)!} \left[\frac{d}{dt} Z_{t, \tau, T}^n \right] Q_{t, \tau, T} dt, \quad \chi_{\tau, T}(I) = \sum_{n=1}^{\infty} \int_0^\tau \frac{(-t)^n Z_{t, \tau, T}^{n-1}}{n!} P_{t, \tau, T} dt$$

where $Q_{t, \tau, T} := DU_t(a_\tau(T-t))$, $Z_{t, \tau, T} := DN(U_t(a_\tau(T-t)))$ and $P_{t, \tau, T} := \partial DU_t(a_\tau(T-t))\dot{a}_\tau(T-t)$ is the Gâteaux derivative of DU_t at $a_\tau(T-t)$ in the direction of $\dot{a}_\tau(T-t)$.

Remark 2.13. In Proposition 2.12, the expansion of the solution $a(\cdot)$ to (2.10) on $[0, T]$ for a constant in time input $I \in L^p(\mathbb{R}^d)$ is obtained by setting $\tau = T$.

Remark 2.14. Proposition 2.12 is stated for $p \in [2, \infty]$, excluding the case $p \in (1, 2)$. While the operators $DN(U_T(a_0))$ and $DN(U_t(a_\tau(T-t)))$ belong to $\mathcal{L}(L^p(\mathbb{R}^d))$ for all $p \in (1, \infty]$, it follows from Proposition B.1 that the operators $\kappa_{\tau, T}(I)$ and $\chi_{\tau, T}(I)$ are well-defined and belong to $\mathcal{L}(L^p(\mathbb{R}^d))$ when $p \in [2, \infty]$.

Remark 2.15. The solution of (2.10) is implicitly represented in both Theorems 2.9 and 2.10. Each representation enables multiple expansion strategies for expressing the final state as a series involving either the initial state a_0 or the final state itself.

From the backward representation (Theorem 2.9):

$$a_\tau(T) = U_T(a_0) + \int_0^T DU_{T-t}(a_\tau(t))I_{sf,\tau}(t) dt = U_T(a_0) + \int_0^\tau DU_t(a_\tau(T-t))I dt,$$

two expansion strategies are possible.

- (i) Using the identity $\int_0^\tau DU_t(a_\tau(T-t))I dt = \int_0^\tau t' DU_t(a_\tau(T-t))I dt$, and applying successive integration by parts, we obtain (F1). This yields the *forward nominal-state* synthesis.
- (ii) Alternatively, using $\int_0^\tau DU_t(a_\tau(T-t))I dt = \int_0^\tau (t-\tau)' DU_T(a_\tau(T-t))I dt$, we derive

$$(F2) \quad a_\tau(T) = U_T(a_0) + \sum_{n=0}^{\infty} \frac{\tau^{n+1} DN(a_\tau(T))^n}{(n+1)!} I - \beta_{\tau,T}(I)I$$

for some operator $\beta_{\tau,T}(I) \in \mathcal{L}(L^p(\mathbb{R}^d))$. This leads to the *forward final-state* synthesis.

From the forward representation (Theorem 2.10):

$$V_T(a_\tau(T)) = a_0 + \int_0^T DV_t(a_\tau(t))I_{sf,\tau}(t) dt = a_0 + \int_0^\tau DV_{T-t}(a_\tau(T-t))I dt,$$

two expansion strategies arise.

- (i) Using $\int_0^\tau DV_{T-t}(a_\tau(T-t))I dt = \int_0^\tau t' DV_{T-t}(a_\tau(T-t))I dt$, we obtain

$$(B1) \quad V_T(a_\tau(T)) = a_0 - \sum_{n=0}^{\infty} \frac{(-\tau)^{n+1} DN(a_0)^n}{(n+1)!} DV_{T-\tau}(U_{T-\tau}(a_0))I - \eta_{\tau,T}(I)I$$

for some operator $\eta_{\tau,T}(I) \in \mathcal{L}(L^p(\mathbb{R}^d))$. This gives rise to the *backward initial-state* synthesis.

- (ii) Alternatively, using $\int_0^\tau DV_{T-t}(a_\tau(T-t))I dt = \int_0^\tau (t-\tau)' DV_{T-t}(a_\tau(T-t))I dt$, we obtain

$$(B2) \quad V_T(a_\tau(T)) = a_0 + \sum_{n=0}^{\infty} \frac{\tau^{n+1} DN(V_T(a_\tau(T)))^n}{(n+1)!} DV_T(a_\tau(T))I - \zeta_{\tau,T}(I)I,$$

for some operator $\zeta_{\tau,T}(I) \in \mathcal{L}(L^p(\mathbb{R}^d))$. This yields the *backward nominal-state* synthesis.

2.2.3. Forward nominal-state synthesis. This section presents the generic synthesis based on the series expansion of the solution to (2.10) given in Proposition 2.12. We provide a detailed analysis of this approach, which serves as a prototypical example of the family of synthesis strategies derived from the dual representations of the solution of (2.10), as discussed in Remark 2.15. The remaining synthesis strategies—the forward final-state, backward initial-state, and backward nominal-state formulations—can be derived through analogous arguments.

The first results are presented in the following theorem. It provides an implicit step-function input that solves the control objective. The proof is presented in Section A.4.

THEOREM 2.16. *Let $p \in [2, \infty]$ and $(a_0, a_1) \in L^p(\mathbb{R}^d)^2$. Let $T \geq \tau$ where $\tau > 0$ be such that the following spectral condition holds*

$$(2.22) \quad \sigma(DN(U_T(a_0))) \cap \left\{ i \frac{2\pi\ell}{\tau} \in \mathbb{C} \mid \ell \in \mathbb{Z} \right\} = \emptyset.$$

Then, the solution $a_\tau(\cdot)$ to (2.10) corresponding to the step-function input $I_{sf,\tau}(\cdot)$ defined in (2.20) satisfies $a_\tau(T) = a_1$, if and only if, $I \in L^p(\mathbb{R}^d)$ satisfies

$$(2.23) \quad [\text{Id} - \mathcal{A}_{\tau,T}(a_0)\varphi_{\tau,T}(I)] I = \mathcal{A}_{\tau,T}(a_0)(a_1 - U_T(a_0))$$

where $\varphi_{\tau,T}(I) \in \mathcal{L}(L^p(\mathbb{R}^d))$ is defined as in Proposition 2.12 and $\mathcal{A}_{\tau,T}(a_0) \in \mathcal{L}(L^p(\mathbb{R}^d))$ is given by

$$(2.24) \quad \mathcal{A}_{\tau,T}(a_0) := DV_\tau(U_T(a_0)) \left[\text{Id} - e^{-\tau DN(U_T(a_0))} \right]^{-1} DN(U_T(a_0)).$$

Remark 2.17. We first refer the reader to Remark 2.14 for a discussion of the restriction to the range $p \in [2, \infty]$. As in the linear case (see Lemma 2.8), the spectral condition in (2.22) is automatically satisfied when $\mu < \mu_0$ —or even $\mu < \mu_1$ when $p = 2$ —as a consequence of Lemma B.3.

By contrast, in the nonlinear setting, it remains unclear whether the implicit equation (2.23), which defines the candidate constant-in-time input, admits at least one solution $I \in L^p(\mathbb{R}^d)$ when the operator $\varphi_{\tau,T}(I)$ is not identically zero. Nevertheless, (2.21) shows that $\varphi_{\tau,T}(I) \equiv 0$ when the transfer function f is linear.

The step-function input synthesis in Theorem 2.16 is implicitly defined in terms of the unknown $I \in L^p(\mathbb{R}^d)$, which may limit the ability of its direct use in practice or numerical implementation. To address this, we now derive an explicit, tractable, and effective approximation of the step-function input synthesized in Theorem 2.16. This approximation offers practical and computational advantages, particularly for numerical implementations.

We begin with the following result, which provides an expansion of $\varphi_{\tau,T}(I)$ as $\tau \rightarrow 0$. The proof is provided in Section A.5.

PROPOSITION 2.18. *Under the assumptions of Theorem 2.16, the following expansion holds*

$$(2.25) \quad \varphi_{\tau,T}(I) = \left[e^{\tau\Phi_T(a_0)} - \text{Id} \right] \Phi_T(a_0)^{-1} \left[e^{-\tau\Phi_T(a_0)} DU_\tau(U_{T-\tau}(a_0)) - \text{Id} \right] + \mathcal{O}(\tau^3), \quad \text{as } \tau \rightarrow 0.$$

where $\Phi_T(a_0) := DN(U_T(a_0))$. In particular, the following expansion also holds

$$(2.26) \quad \text{Id} - \mathcal{A}_{\tau,T}(a_0)\varphi_{\tau,T}(I) = DV_\tau(U_T(a_0))e^{-\tau\Phi_T(a_0)} + \mathcal{O}(\tau^2), \quad \text{as } \tau \rightarrow 0.$$

The following result provides an explicit input synthesis along with an estimate of the endpoint error.

THEOREM 2.19. *Let $p \in [2, \infty]$ and $(a_0, a_1) \in L^p(\mathbb{R}^d)^2$. Let $T \geq \tau$ where $\tau > 0$ be such that the spectral condition (2.22) is satisfied. Define $I_{fn} \in L^p(\mathbb{R}^d)$ by*

$$(2.27) \quad I_{fn} = \left[e^{\tau DN(U_T(a_0))} - \text{Id} \right]^{-1} DN(U_T(a_0))(a_1 - U_T(a_0)).$$

Then, the solution $a_\tau(\cdot)$ to (2.10) corresponding to the step-function input $\tilde{I}_{sf,\tau} : [0, T] \rightarrow L^p(\mathbb{R}^d)$,

$$(2.28) \quad \tilde{I}_{sf,\tau}(t) = \begin{cases} 0 & \text{if } 0 \leq t \leq T - \tau \\ I_{fn} & \text{if } T - \tau < t \leq T \end{cases}$$

satisfies the following endpoint error estimates

$$(2.29) \quad \|a_\tau(T) - a_1\|_p = \mathcal{O}(\tau^2), \quad \text{as } \tau \rightarrow 0.$$

Remark 2.20. We emphasize that the constant-in-time input synthesized in Theorem 2.19 corresponds to the special case $T = \tau$. The notation I_{fn} in (2.27) stands for *forward nominal* synthesis, where “nominal” refers to the evaluation of $DN(\cdot)$ along the nominal trajectory $U_t(a_0)|_{t=T}$ of (2.10).

Proof of Theorem 2.19. Using (F1), (2.25), and the definition of I_{fn} from (2.27), we obtain

$$(2.30) \quad \begin{aligned} a_\tau(T) &= U_T(a_0) - \sum_{n=0}^{\infty} \frac{(-\tau)^{n+1} \Phi_T(a_0)^n}{(n+1)!} DU_\tau(U_{T-\tau}(a_0)) I_{fn} - \varphi_{\tau,T}(I_{fn}) I_{fn} \\ &\underset{\tau \sim 0}{=} \left[e^{\tau\Phi_T(a_0)} - \text{Id} \right] \Phi_T(a_0)^{-1} \left[e^{\tau\Phi_T(a_0)} - \text{Id} \right]^{-1} \Phi_T(a_0)(a_1 - U_T(a_0)) + \mathcal{O}(\tau^2) \underset{\tau \sim 0}{=} a_1 + \mathcal{O}(\tau^2) \end{aligned}$$

since $\Phi_T(a_0)^{-1}$ commutes with $e^{\tau\Phi_T(a_0)}$ and $e^{-\tau\Phi_T(a_0)}$, where $\Phi_T(a_0) := DN(U_T(a_0))$. Moreover, $\mathcal{O}(\tau^3)$ term in (2.25) becomes $\mathcal{O}(\tau^2)$ in (2.30) due to the relation $\left[e^{\tau\Phi_T(a_0)} - \text{Id} \right]^{-1} \mathcal{O}(\tau^3) \underset{\tau \sim 0}{=} \mathcal{O}(\tau^2)$, since $\Phi_T(a_0)$ is uniformly bounded with respect to T and a_0 so that $\left[e^{\tau\Phi_T(a_0)} - \text{Id} \right]^{-1} \underset{\tau \sim 0}{=} \mathcal{O}(\tau^{-1})$. \square

Remark 2.21. Observe that (2.26) ensures that (2.23) admits the solution $I \in L^p(\mathbb{R}^d)$ given by

$$\begin{aligned} I &= e^{\tau \Phi_T(a_0)} [DV_\tau(U_T(a_0))]^{-1} \mathcal{A}_{\tau,T}(a_0) (a_1 - U_T(a_0)) + \mathcal{O}(\tau^2) \quad \text{as } \tau \rightarrow 0 \\ &= I_{fn} + \mathcal{O}(\tau^2) \quad \text{as } \tau \rightarrow 0 \end{aligned}$$

where $I_{fn} \in L^p(\mathbb{R}^d)$ is given by (2.27).

3. Generic syntheses in practice. Building on the implicit forward nominal-state synthesis and its explicit approximation developed in Section 2.2.3, this section extends the analysis to the forward final-state, backward initial-state, and backward nominal-state formulations. Section 3.2 then discusses the spectral conditions needed for these syntheses and shows that they are naturally satisfied in many practical scenarios.

From here on, we focus exclusively on constant-in-time input syntheses, corresponding to the specific case $T = \tau > 0$ as defined in Proposition 2.12 and Section 2.2.3.

3.1. Explicit approximations for the remaining syntheses. This section provides explicit approximations for the forward final-state, backward initial-state, and backward nominal-state syntheses, derived from the solution expansions in (F2), (B1), and (B2). The next proposition summarizes these three syntheses. The proof follows the same lines as Theorem 2.19 and is omitted for brevity.

PROPOSITION 3.1. *Let $p \in [2, \infty]$, $(a_0, a_1) \in L^p(\mathbb{R}^d)^2$ and $T > 0$. Then, one has:*

1. *If the following spectral condition is satisfied*

$$(3.1) \quad \sigma(DN(a_1)) \cap \left\{ i \frac{2\pi\ell}{T} \in \mathbb{C} \mid \ell \in \mathbb{Z} \right\} = \emptyset$$

then, the solution $a_f(\cdot)$ to (2.10) corresponding to the input $I_f \in L^p(\mathbb{R}^d)$ given by

$$(3.2) \quad I_f = \left[e^{TDN(a_1)} - \text{Id} \right]^{-1} DN(a_1)(a_1 - U_T(a_0))$$

satisfies $\|a_f(T) - a_1\|_p = \mathcal{O}(T^2)$ as $T \rightarrow 0$.

2. *If the following spectral condition is satisfied*

$$(3.3) \quad \sigma(DN(a_0)) \cap \left\{ i \frac{2\pi\ell}{T} \in \mathbb{C} \mid \ell \in \mathbb{Z} \right\} = \emptyset$$

then, the solution $a_b(\cdot)$ to (2.10) corresponding to the input $I_b \in L^p(\mathbb{R}^d)$ given by

$$(3.4) \quad I_b = \left[\text{Id} - e^{-TDN(a_0)} \right]^{-1} DN(a_0)(V_T(a_1) - a_0)$$

satisfies $\|a_b(T) - a_1\|_p = \mathcal{O}(T^2)$ as $T \rightarrow 0$.

3. *If the following spectral condition is satisfied*

$$(3.5) \quad \sigma(DN(V_T(a_1))) \cap \left\{ i \frac{2\pi\ell}{T} \in \mathbb{C} \mid \ell \in \mathbb{Z} \right\} = \emptyset$$

then, the solution $a_{bn}(\cdot)$ to (2.10) corresponding to the input $I_{bn} \in L^p(\mathbb{R}^d)$ given by

$$(3.6) \quad I_{bn} = \left[\text{Id} - e^{-TDN(V_T(a_1))} \right]^{-1} DN(V_T(a_1))(V_T(a_1) - a_0)$$

satisfies $\|a_{bn}(T) - a_1\|_p = \mathcal{O}(T^2)$ as $T \rightarrow 0$.

Remark 3.2. The four synthesized inputs I_{fn} , I_f , I_b , and I_{bn} —defined respectively by equations (2.27), (3.2), (3.4), and (3.6)—never coincide in general. This can be seen even in the trivial case where the initial state a_0 is an equilibrium of the drift dynamics $\dot{a}(t) = N(a(t))$, i.e., $N(a_0) = 0$.

In this situation, it is clear that $U_T(a_0) = a_0$ and $DN(U_T(a_0)) = DN(a_0)$ so that I_b and I_{bn} remain as defined in (3.4) and (3.6), while the forward nominal-state and final-state syntheses recast

$$I_{fn} = \left[e^{T DN(a_0)} - \text{Id} \right]^{-1} DN(a_0)(a_1 - a_0), \quad I_f = \left[e^{T DN(a_1)} - \text{Id} \right]^{-1} DN(a_1)(a_1 - a_0).$$

This clearly shows that the four control inputs are distinct. The only overlap occurs in the spectral conditions: I_{fn} and I_b are both well-defined under the same spectral condition (3.3), which is generally not the case when $N(a_0) \neq 0$ (see Proposition 3.4 below).

Furthermore, if a_1 is also an equilibrium⁵ of the drift, then $V_T(a_1) = a_1$, $DN(V_T(a_1)) = DN(a_1)$, and

$$I_b = \left[\text{Id} - e^{-T DN(a_0)} \right]^{-1} DN(a_0)(a_1 - a_0), \quad I_{bn} = \left[\text{Id} - e^{-T DN(a_1)} \right]^{-1} DN(a_1)(a_1 - a_0).$$

Note, in particular, that I_f and I_{bn} are now well-defined under the same spectral condition (3.1). Altogether, even in this special case where both a_0 and a_1 are equilibria of the drift, we still have $I_{fn} \neq I_f \neq I_b \neq I_{bn}$.

3.2. On the spectral conditions and beyond. Here, we analyze the spectral conditions underlying the validity of each synthesis strategy. To begin this section, we state the following informative remark.

Remark 3.3. It follows from Lemma B.4 that

$$DN(U_T(a)) = DU_T(a) DN(a) DU_T(a)^{-1} + \partial DU_T(a) N(a) DU_T(a)^{-1}, \quad a \in L^p(\mathbb{R}^d).$$

Then, $\mathcal{B} := DU_T(a) DN(a) DU_T(a)^{-1}$ is congruent to $DN(a)$ so that $\sigma(\mathcal{B}) = \sigma(DN(a))$. Next, the operator $\partial DU_T(a) N(a) DU_T(a)^{-1}$ vanishes identically only when either $N(a) = 0$ or $T = 0$, since $\partial DU_T(a)|_{T=0} = 0$. Therefore, we deduce that for any $a \in L^p(\mathbb{R}^d)$ with $N(a) \neq 0$, it holds

$$\sigma(DN(U_T(a))) \neq \sigma(DN(a)), \quad \forall T > 0.$$

Nevertheless, the following result shows that these spectra remain close in a precise sense, as established through perturbation theory for bounded linear operators [31, p. 208] and the fact that

$$(3.7) \quad \|\partial DU_T(a) N(a) DU_T(a)^{-1}\|_{\mathcal{L}(L^p(\mathbb{R}^d))} = \mathcal{O}(T) \quad \text{as } T \rightarrow 0$$

by Lemma B.2.

PROPOSITION 3.4. *Let $p \in [2, \infty]$, $a \in L^p(\mathbb{R}^d)$, and $T \geq 0$. Then, the following holds*

$$(3.8) \quad \sigma(DN(U_T(a))) \subseteq \sigma(DN(a)) + \mathcal{O}(T) \quad \text{as } T \rightarrow 0.$$

In particular, $\sigma(DN(U_T(a))) = \sigma(DN(a))$, if and only if, either $N(a) = 0$ or $T = 0$.

We recall from Lemma 2.8 and Remark 2.17 that these spectral conditions are automatically satisfied when

$$(\mu < \mu_0 \text{ if } 2 \leq p \leq \infty) \quad \text{or} \quad (\mu < \mu_1 \text{ if } p = 2)$$

where the threshold parameters $0 < \mu_0 \leq \mu_1$ are introduced in (1.5). The main challenge lies in verifying the spectral conditions in the critical or supercritical regime, i.e., when $\mu \geq \mu_0$ or $\mu \geq \mu_1$ (in the case $p = 2$).

In the specific case of a constant $a \in L^\infty(\mathbb{R}^d)$, one has the following result, where the proof can be done by invoking classical Fourier transform arguments.

⁵This scenario is of practical interest—for example, when the goal is to drive the neural field from an unstable equilibrium a_0 to a stable equilibrium a_1 using constant in time input.

PROPOSITION 3.5. *Assume that*

$$(3.9) \quad \omega(-x) = \omega(x), \quad \forall x \in \mathbb{R}^d.$$

If $a \in L^\infty(\mathbb{R}^d)$ is constant (e.g., the homogeneous stationary state of $\dot{a}(t) = N(a(t))$), then $DN(a) \in \mathcal{L}(L^2(\mathbb{R}^d))$ is self-adjoint, and its spectrum is given by

$$(3.10) \quad \sigma(DN(\bar{a})) = \left[-\alpha + \mu f'(a) \min_{\xi \in \mathbb{R}^d} \widehat{\omega}(\xi), -\alpha + \mu f'(a) \max_{\xi \in \mathbb{R}^d} \widehat{\omega}(\xi) \right] \subset \mathbb{R}.$$

Remark 3.6. The symmetry assumption (3.9) is standard in the literature, as most neural field models on unbounded domains \mathbb{R} or \mathbb{R}^2 typically use kernels that are both homogeneous and isotropic, meaning $\omega(x, y) = \omega(|x - y|)$ [10, 12, 50, 51, 18, 27, 39, 34]. It is relevant to ensure that $\sigma(DN(a)) \subset \mathbb{R}$ when a is real constant. It follows from (3.10) that the spectral conditions (2.22), (3.1), (3.3), and (3.5) are violated if and only if $0 \in \sigma(DN(\bar{a}))$ in the case where $a_0 = \bar{a}$, $a_1 = \bar{a}$, $U_T(a_0) = \bar{a}$ or $V_T(a_1) = \bar{a}$. This occurs if and only if

$$\mu = \frac{\alpha}{f'(\bar{a})\lambda}, \quad \text{for some } \lambda \in \left[\min_{\xi \in \mathbb{R}^d} \widehat{\omega}(\xi), \max_{\xi \in \mathbb{R}^d} \widehat{\omega}(\xi) \right].$$

4. Comments on the generic syntheses and perspectives. This section discusses the generic syntheses developed in Sections 2.2 and 3, outlining their complementarity, practical limitations, and possible directions for future investigation.

As already noted in Remark 2.14, the restriction to the range $2 \leq p \leq \infty$ in the main results stated in Proposition 2.12, Theorems 2.16 and 2.19, and Proposition 3.1, involves a subtle technical consideration. While the operator $DN(a) \in \mathcal{L}(L^p(\mathbb{R}^d))$ is indeed well-defined for all $1 < p \leq 2$ by [50, Lemma B.8], the operator $\varphi_{\tau, T}(I) \in \mathcal{L}(L^p(\mathbb{R}^d))$ involves the Gâteaux derivative ∂DN of the Fréchet derivative DN under the integral sign. However, Proposition B.1 only guarantees that $\partial DN(h)k \in \mathcal{L}(L^p(\mathbb{R}^d))$ for all $h, k \in L^p(\mathbb{R}^d)$ if $p \in [2, \infty]$.

This raises an open question: is DN Gâteaux differentiable on $L^p(\mathbb{R}^d)$ for $p \in (1, 2)$? An affirmative answer would extend the validity of the proposed input syntheses to the full range $p \in (1, \infty]$. We refer to Remark 2.11 for the specific case of $p = 1$.

The proposed input syntheses (2.27), (3.2), (3.4), and (3.6) apply to a broad class of nonlinear dynamical systems of the form (2.10), namely

$$\dot{a}(t) = N(a(t)) + I,$$

where $a(t)$ evolves in a Banach space \mathcal{X} , and the drift $N \in C^1(\mathcal{X})$, the Fréchet derivative DN is Gâteaux differentiable, and the following uniform boundedness conditions are satisfied: there exists $C > 0$ such that

$$\sup_{u \in \mathcal{X}} \|DN(u)\| \leq C, \quad \sup_{u \in \mathcal{X}} \|\partial DN(u)\| \leq C.$$

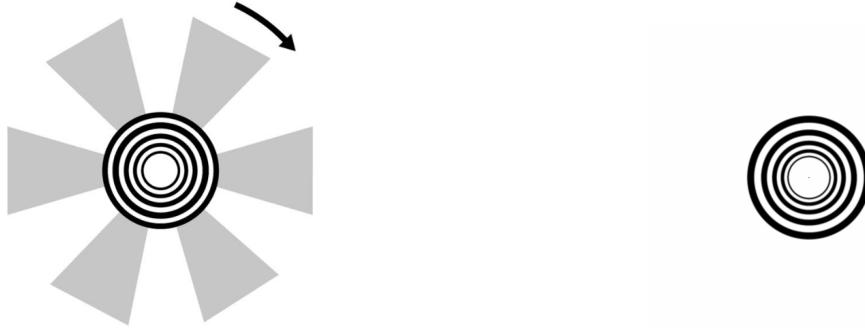
Finally, we emphasize that our proposed constant-in-time input syntheses do not directly extend to neural field models written in the *activity-based* form [11, 23, 25, 35], namely

$$(4.1) \quad \partial_t a(x, t) = -\alpha a(x, t) + \mu f([\omega * a](x, t) + I(x)), \quad a(x, 0) = a_0(x), \quad (x, t) \in \mathbb{R}^d \times \mathbb{R}_+.$$

A detailed analysis of the extension of the proposed synthesis to (4.1) is left for future work.

5. How can the syntheses be used to predict visual illusions?. Visual illusions are striking phenomena that shed light on the intricate workings of the visual system. It is well established that the visual system can produce illusory colors and shapes absent from the actual stimulus [29]. Such illusions arise from specific patterns of neural activity—typically resulting from dynamic interactions within the visual cortex—and they often emerge almost instantaneously following exposure to a visual stimulus [8, 9, 36, 37].

In modeling experimentally observed visual illusions using neural dynamics, the prevailing approach in the literature—see, e.g., [10, 39, 49, 50, 51]—relies on the stationary version of (2.10). In this framework, illusory



(a) Geometrical pattern v_T to induce in the visual field. The arrow indicates the direction of apparent motion [8]. (b) Visual stimulus v_I that induces the illusion v_T in Fig. 1a, as reported in [8].

perceptual patterns are interpreted as the inverse retinotopic image of a steady-state cortical activity profile driven by a visual stimulus via a corresponding sensory input.

This mechanistic approach offers a clear and interpretable link between the stimulus and the resulting perception. It is naturally suited to scenarios where the illusion emerges after the dynamics have stabilized, i.e., in the asymptotic regime, which is often appropriate given that many visual illusions can persist in the visual field for several seconds, see, for instance, [37]. That said, several well-known illusions—including the visual MacKay effect (especially for the “MacKay target”) [37], the phenomena studied by Billock and Tsou [8], the Fraser spiral illusion [28], and the café wall illusion [33]—can be perceived within very short (approximately 10 sec. for the visual MacKay effect from the “MacKay ray” visual stimulus [37]) latencies following stimulus onset. In such cases, cortical dynamics remain far from equilibrium, and the initial state of neural activity—modeled as a_0 in equation (NF)—may significantly influence the illusory experience.

In this application, we should assume that the dimension of the space variable is $d = 2$. As a prototypical example, suppose we aim to design a visual input v_I that induces the perceptual pattern shown in Fig. 1a—denoted by v_T —after T seconds of observation. This approach explicitly accounts for the initial cortical state, which can strongly influence the resulting perception. The pattern in Fig. 1a was originally reported in the psychophysical experiments of [8], where localized oriented stimuli in the visual field were shown to evoke compelling illusory perceptions in surrounding regions after brief exposures.

The control-theoretic formulation is as follows: Let $T > 0$ denote the small target time at which the illusory percept v_T is observed. Let $a_1 := \mathcal{R}v_T$ represent the corresponding V1 cortical activity, obtained via the retinotopic map \mathcal{R} (see, e.g., [12, 44]) between the visual field (retina) and V1, and let a_0 denote the initial cortical state in V1. If we assume that the average activity in V1 evolves according to (NF) (when neglecting the label that models V1’s functional features, e.g., the sensitivity of V1’s “simple cells” to local orientations from the stimuli in the retina [12]), the goal is to synthesize a constant-in-time input I such that the solution $a(\cdot)$ to (NF) satisfies $\|a(\cdot, T) - a_1\|_p \leq \varepsilon$ for a prescribed small $\varepsilon > 0$ in a suitable $L^p(\mathbb{R}^2)$ norm. The corresponding visual stimulus is then obtained via the inverse retinotopic map as $v_I = \mathcal{R}^{-1}I$.

Since a_1 is fixed and I can be synthesized using any of the formulations (2.27), (3.2), (3.4), or (3.6), the primary degree of freedom—aside from the intrinsic parameters ω , f , μ , and α in (NF), which also influence the synthesis—is the choice of the initial state a_0 . For example, in the case of the target pattern v_T in Fig. 1a, [8] provides a stimulus v_I —depicted in Fig. 1b—known to induce this illusion. Therefore, the input I is said to predict a visual illusion if its inverse retinotopic map coincides with an experimentally validated visual stimulus.

We defer to future work the application of the proposed syntheses for predicting visual illusions, as outlined in this section. This endeavor will require collaboration with researchers in visual perception science to experimentally validate the synthesized inputs, following approaches similar to those in [8].

6. Numerical illustration of the proposed constant-in-time input syntheses. This section presents numerical illustrations of the control syntheses developed in Section 2.2, implemented in the scientific computing

language `Julia` [7, 32]. Our goal is to demonstrate their practical effectiveness through simulations on one- and two-dimensional spatial domains. Specifically, we consider the approximate constant-in-time inputs $I_{fn}(\cdot)$, $I_f(\cdot)$, $I_b(\cdot)$, and $I_{bn}(\cdot)$ —defined for a short time horizon $T = \tau > 0$ by equations (2.27), (3.2), (3.4), and (3.6), respectively—and solve (NF) under each input to obtain the corresponding final states $a_{fn}(\cdot, T)$, $a_f(\cdot, T)$, $a_b(\cdot, T)$, and $a_{bn}(\cdot, T)$. We then evaluate the endpoint errors

$$(6.1) \quad \|a_{fn}(\cdot, T) - a_1(\cdot)\|_p, \quad \|a_f(\cdot, T) - a_1(\cdot)\|_p, \quad \|a_b(\cdot, T) - a_1(\cdot)\|_p, \quad \text{and} \quad \|a_{bn}(\cdot, T) - a_1(\cdot)\|_p,$$

in the $L^p(\mathbb{R}^d)$ norm to verify that they remain small, consistent with the theoretical guarantees.

To assess the accuracy and efficiency of the proposed generic syntheses, we also compare (see Fig. 3) them to standard input syntheses based on the linearization of the nonlinear equation (2.10) about the initial and target states, a_0 and a_1 , respectively. The corresponding linearized inputs are given by

$$(6.2) \quad \begin{aligned} I_{a_0} &= -N(a_0) + \left[e^{TDN(a_0)} - \text{Id} \right]^{-1} DN(a_0)(a_1 - e^{TDN(a_0)}a_0), \\ I_{a_1} &= -N(a_1) + \left[e^{TDN(a_1)} - \text{Id} \right]^{-1} DN(a_1)(a_1 - e^{TDN(a_1)}a_0), \end{aligned}$$

and the corresponding solutions to (2.10) are denoted $a_{a_0}(\cdot)$ and $a_{a_1}(\cdot)$. Observe that $I_{a_0} = I_{fn}$ and $I_{a_1} = I_{bn}$ if both a_0 and a_1 are equilibria of the drift dynamics $\dot{a}(t) = N(a(t))$.

All simulations are performed in `Julia` using the `DifferentialEquations` package, where (NF) is integrated via the `solve` routine. The convolution kernel is constructed using `centered` and `imfilter` functions from the `ImageFiltering` package. To compute the Jacobian-vector product $DN(a)b$, rather than relying on finite-difference approximations as commonly suggested in [32]—which may introduce numerical inaccuracies—we employ automatic differentiation via the `ForwardDiff` package. To evaluate $e^{TDN(a)}$, we construct the Jacobian matrix $DN(a)$ by applying it to each canonical basis vector e_i of \mathbb{R}^M , where M is the number of spatial discretization points.

Finally, it is worth noting that the parameter $\mu > 0$ in each example is expressly chosen in such a way that Theorem 2.4 cannot be applied.

6.1. Examples in a one-dimensional spatial domain. As noted in the introduction, this example is biologically motivated: it demonstrates that a bump-like activity pattern—commonly associated with neural encoding in working or short-term memory [34]—can be successfully induced over a short time horizon $T = 0.25$, even in a subcritical regime $\mu < \mu_c$, where such patterns do not naturally arise.

To this end, we consider the Amari-type neural field equation (NF) posed on a one-dimensional domain, with parameters drawn from [27]:

$$(6.3) \quad \omega(x) = 2\hat{\omega}_c(\hat{\omega}_c + 1)e^{-|x|} - \frac{(2\hat{\omega}_c + 1)^2}{2} \sqrt{\frac{\hat{\omega}_c}{\hat{\omega}_c + 1}} e^{-\sqrt{\frac{\hat{\omega}_c}{\hat{\omega}_c + 1}}|x|}, \quad f(x) = \frac{1}{1 + \exp(-x + \theta)} - \frac{1}{1 + \exp(\theta)},$$

where $\hat{\omega}_c := \max_{\xi \in \mathbb{R}} \hat{\omega}(\xi) = \hat{\omega}(\pm 1/2\pi) = 5$ and $\theta = 3.5$. Note also from [27] that $\hat{\omega}(0) = \min_{\xi \in \mathbb{R}} \hat{\omega}(\xi) = -1$.

According to [27], in the absence of external input, the trivial state $a \equiv 0$ is the unique exponentially stable equilibrium for $\mu < \mu_c$, and a bifurcation occurs at $\mu = \mu_c$. At this point, two symmetric branches of spatially localized solutions emerge, which are approximately given by

$$a(x) = 2\sqrt{\frac{-2c_1^1\lambda}{c_3^0}} \operatorname{sech}\left(x\sqrt{c_1^1\lambda}\right) \cos(x + \phi) + \mathcal{O}(\lambda), \quad x \in \mathbb{R},$$

for small $\lambda < 0$, where $\phi \in \{0, \pi\}$, and $c_1^1, c_3^0 < 0$ are constants depending on f , ω , and μ_c .

For the simulations, we fix $\phi = 0$, neglect higher-order terms in λ , and assume $c_1^1\lambda = 0.0625$ and $c_3^0 = -2$. The initial and target states are defined as

$$(6.4) \quad a_0(x) = 0, \quad a_1(x) = 0.5 \operatorname{sech}(0.25x) \cos(x), \quad x \in \mathbb{R},$$

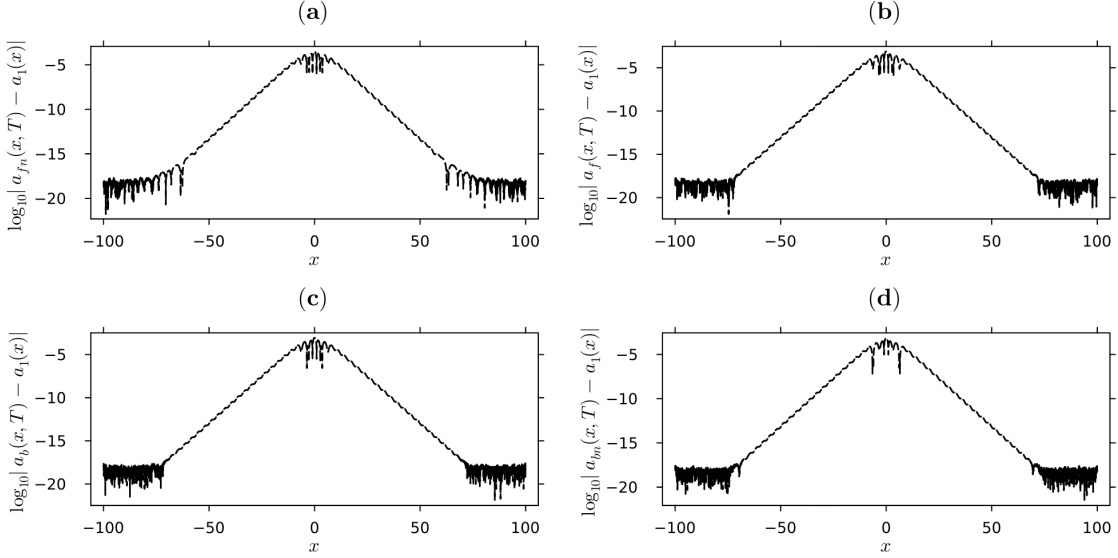


Fig. 2: Log-scale plot of the endpoint mismatch $\log_{10}|a(x, T) - a_1(x)|$ for each of the four control strategies, with a_0 and a_1 defined in (6.4) and final time $T = 0.25$. **(a)** Forward nominal-state input: $\|a_{fn}(\cdot, T) - a_1(\cdot)\|_2 = 4.4 \times 10^{-4}$, $\|a_{fn}(\cdot, T) - a_1(\cdot)\|_\infty = 3.3 \times 10^{-4}$. **(b)** Forward final-state input: $\|a_f(\cdot, T) - a_1(\cdot)\|_2 = 9.9 \times 10^{-4}$, $\|a_f(\cdot, T) - a_1(\cdot)\|_\infty = 7.9 \times 10^{-4}$. **(c)** Backward initial-state input: $\|a_b(\cdot, T) - a_1(\cdot)\|_2 = 1.1 \times 10^{-3}$, $\|a_b(\cdot, T) - a_1(\cdot)\|_\infty = 8.8 \times 10^{-4}$. **(d)** Backward nominal-state input: $\|a_{bn}(\cdot, T) - a_1(\cdot)\|_2 = 9.4 \times 10^{-4}$, $\|a_{bn}(\cdot, T) - a_1(\cdot)\|_\infty = 7.7 \times 10^{-4}$. The mismatch is sharply localized around $x = 0$, where the target bump is centered and where the derivatives $f'(U_T(a_0))$, $f'(a_1)$, $f'(a_0)$, and $f'(V_T(a_1))$ reach their maximum values, amplifying sensitivity to perturbations. Here ω and f are given in (6.3).

both belonging to $L^2(\mathbb{R}) \cap L^\infty(\mathbb{R})$. As in [27], we set $\alpha = 1$. Then, by Remark 3.6 and the definition of μ_c in (1.5), the inputs I_{fn} and I_b are well defined whenever

$$\mu \in (0, \mu_c) = (0, 7.02).$$

Likewise, by Remark 2.17 and the definition of μ_1 in (1.5), the inputs I_f and I_{bn} are well defined if

$$\mu \in (0, \mu_1) = (0, 0.8).$$

To ensure uniform applicability across all synthesis strategies, we set $\mu = 0.625 \mu_1 = 0.5$ in the experiments.

For implementation, the spatial domain $\Omega = [-L, L]$ with $L = 100$ is discretized with mesh width $\Delta x = 0.025$, yielding $M = 1 + \frac{2L}{\Delta x} = 8001$ uniformly spaced grid points. To assess the effectiveness of each control, we compute the endpoint errors (6.1) over Ω in both the L^2 and L^∞ norms. See Fig. 2 for detailed results.

In the second example, we consider the neural field equation (NF) on \mathbb{R} with a Difference-of-Gaussians (DoG) connectivity kernel and a shifted sigmoid activation function

$$(6.5) \quad \omega(x) = \frac{1}{\sigma_1 \sqrt{2\pi}} e^{-\frac{x^2}{2\sigma_1^2}} - \frac{\kappa}{\sigma_2 \sqrt{2\pi}} e^{-\frac{x^2}{2\sigma_2^2}}, \quad f(x) = \frac{1}{1 + e^{-x+0.25}} - \frac{1}{1 + e^{0.25}}, \quad x \in \mathbb{R},$$

with parameters $\sigma_1 = 1/(\pi\sqrt{2})$, $\sigma_2 = \sqrt{2}/\pi$, and $\kappa = 0.95$. We set $\alpha = 0.1$ and $\mu = 0.75\mu_1 = 0.624$, where $\mu_1 = 0.832 < \mu_c = 0.845$ is computed using (1.5). The initial and target states are defined by

$$(6.6) \quad a_0(x) = \frac{1}{\sqrt{1+x^2}}, \quad a_1(x) = e^{-x^2} - 0.5e^{-0.5x^2}, \quad x \in \mathbb{R},$$

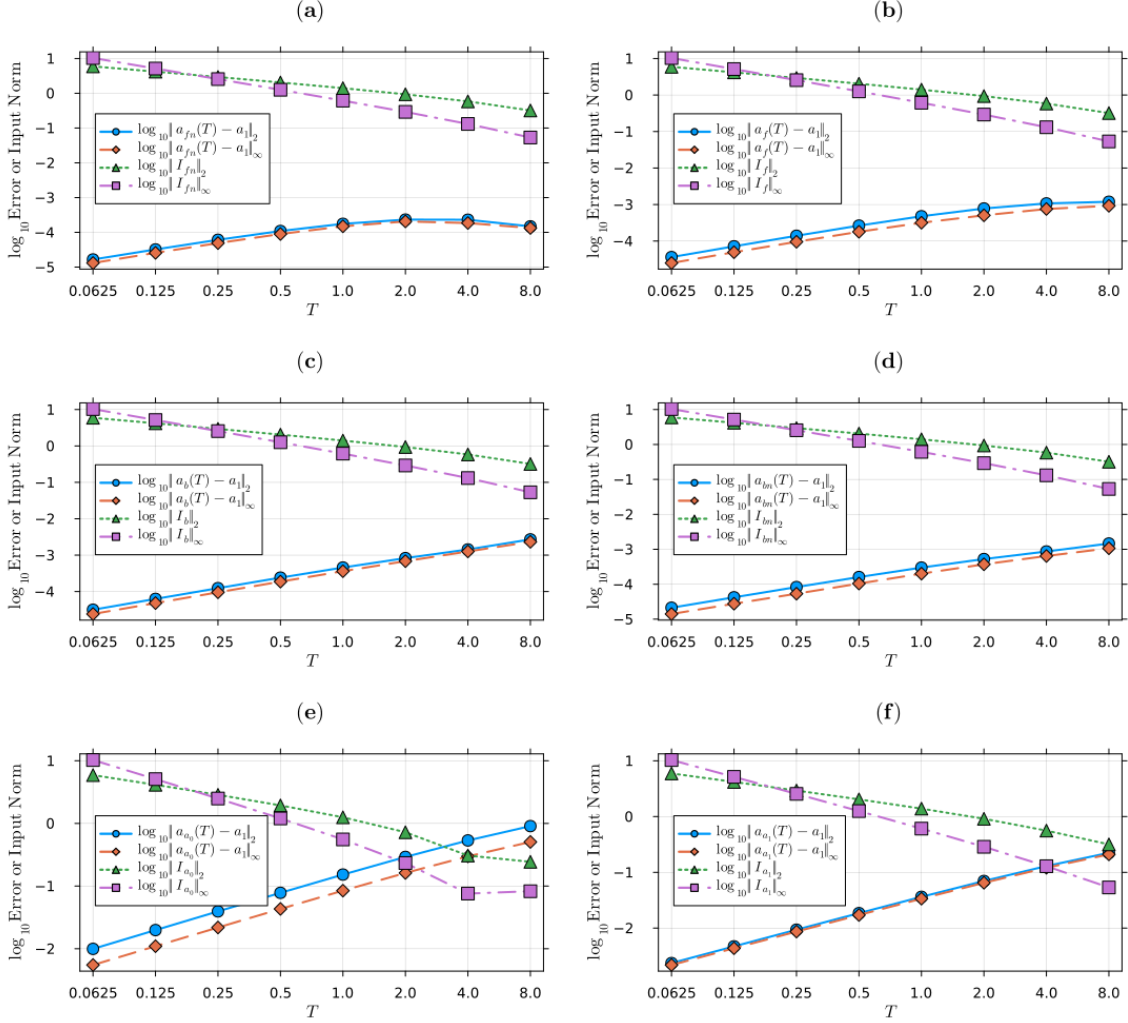


Fig. 3: Comparison of \log_{10} endpoint errors and input norms for each control synthesis strategy as a function of the time horizon $T \in \{0.0625, 0.125, 0.25, 0.5, 1, 2, 4, 8\}$, with ω and f defined in (6.5) and a_0, a_1 given in (6.6), satisfying $\|a_1 - a_0\|_{L^2(\Omega)} = 1.49$ and $\|a_1 - a_0\|_{L^\infty(\Omega)} = 0.65$. Each panel shows the \log_{10} of the $L^2(\Omega)$ and $L^\infty(\Omega)$ endpoint errors and input norms for: (a) forward nominal-state input I_{fn} , (b) forward final-state input I_f , (c) backward initial-state input I_b , (d) backward nominal-state input I_{bn} , (e) input linearized at the initial state I_{a_0} , (f) input linearized at the target state I_{a_1} . As T increases, the input norms generally decrease for all syntheses except I_{a_0} , which decreases up to $T = 4$ and then rises. For small time horizons, the forward and backward nominal-state syntheses yield the lowest endpoint errors, followed by the backward initial-state and forward final-state syntheses. Notably, both linearized inputs I_{a_0} and I_{a_1} given in (6.2) perform significantly worse than the generic syntheses in terms of both error and input norm.

both of which belong to $L^2(\mathbb{R}) \cap L^\infty(\mathbb{R})$. According to Amari’s terminology [2], the initial state a_0 can be interpreted as an “ ∞ -solution” corresponding to a spatially widespread excitation across the entire domain, while the target state a_1 represents a “1-bump” solution, characterized by a localized region of activity.

Under this setting, all constant-in-time inputs I_{fn} , I_f , I_b , I_{bn} , I_{a_0} , and I_{a_1} are well-defined. For simulations, the spatial domain $\Omega = [-L, L]$ with $L = 20$ is discretized using a uniform mesh with step size $\Delta x = 0.01$,

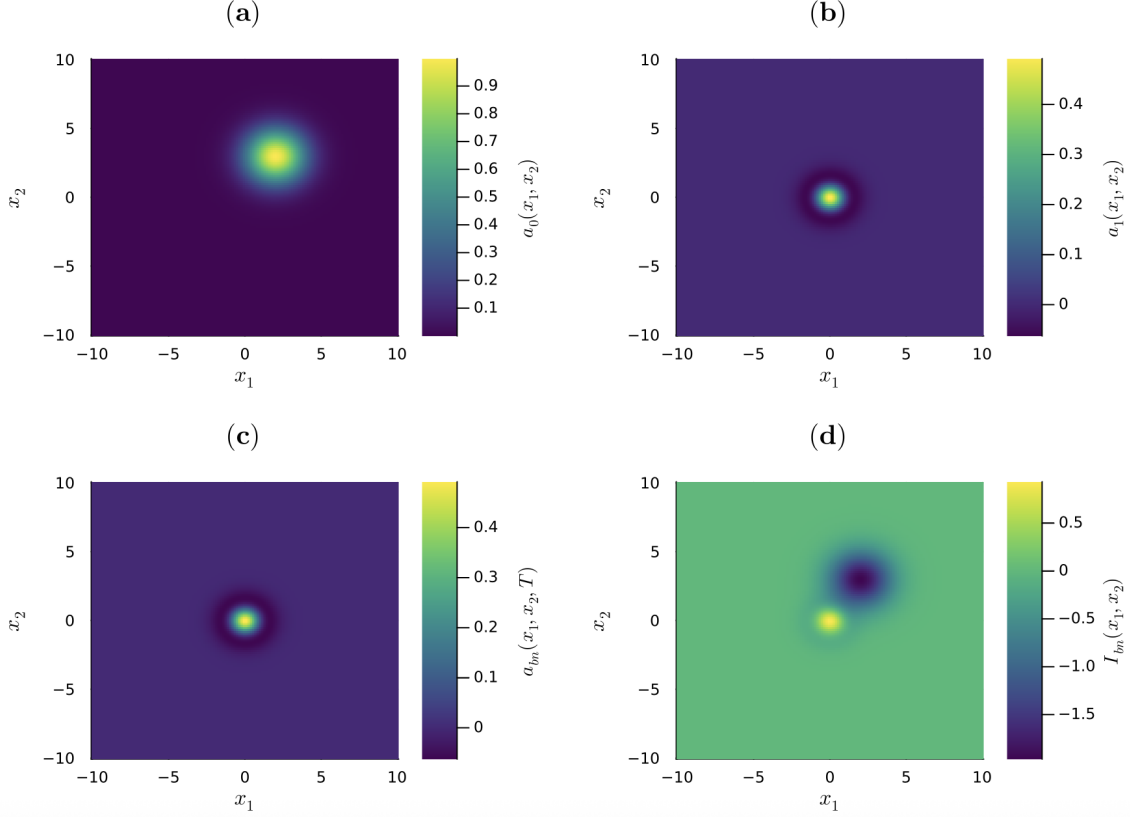


Fig. 4: Numerical simulation of the two-dimensional neural field model (NF) controlled via the backward nominal-state input I_{bn} over the time horizon $T = 0.5$, using parameters from (6.7) and initial/target states from (6.8). (a) Initial state $a_0(x_1, x_2)$. (b) Target state $a_1(x_1, x_2)$. (c) Final state $a_{bn}(x_1, x_2, T)$. (d) Input $I_{bn}(x_1, x_2)$ used throughout $[0, T]$. The endpoint errors are $\|a_{bn}(T) - a_1\|_2 = 1.7 \times 10^{-4}$ and $\|a_{bn}(T) - a_1\|_\infty = 8.4 \times 10^{-5}$, while the input norms are $\|I_{bn}\|_2 = 5.05$ and $\|I_{bn}\|_\infty = 1.96$. For reference, the initial discrepancy is $\|a_1 - a_0\|_2 = 2.57$ and $\|a_1 - a_0\|_\infty = 0.99$.

yielding $M = 1 + \frac{2L}{\Delta x} = 4001$ grid points. To evaluate the performance of each control strategy, we compute the endpoint errors $\log_{10} \|a(\cdot, T) - a_1\|_2$ and $\log_{10} \|a(\cdot, T) - a_1\|_\infty$, along with the norms of the corresponding inputs across various time horizons $T \in \{0.0625, 0.125, 0.25, 0.5, 1, 2, 4, 8\}$. We refer to Fig. 3 for visualization.

6.2. Example in two-dimensional spatial domain. We now consider (NF) posed on \mathbb{R}^2 with a difference-of-Gaussians (DoG) lateral connectivity kernel and a shifted sigmoid activation function

$$(6.7) \quad \omega(x) = \frac{1}{2\pi\sigma_1^2} e^{-\frac{|x|^2}{2\sigma_1^2}} - \frac{\kappa}{2\pi\sigma_2^2} e^{-\frac{|x|^2}{2\sigma_2^2}}, \quad f(s) = \frac{1}{1 + e^{-s+0.25}} - \frac{1}{1 + e^{0.25}}, \quad (x, s) \in \mathbb{R}^2 \times \mathbb{R},$$

with parameters $\sigma_1 = 1/(\pi\sqrt{2})$, $\sigma_2 = \sqrt{2}/\pi$, and $\kappa = 0.85$. The objective is to steer the system from the initial state a_0 to the target state a_1 in time $T = 0.5$, where

$$(6.8) \quad a_0(x) = e^{-\left(\frac{(x_1-2)^2}{4} + \frac{(x_2-3)^2}{4}\right)}, \quad a_1(x) = e^{-|x|^2} - 0.5 e^{-\frac{|x|^2}{2}}, \quad x = (x_1, x_2) \in \mathbb{R}^2,$$

both belong to $L^p(\mathbb{R}^2)$. We fix $\alpha = 0.1$ and choose $\mu := 0.75\mu_1 = 0.6$, where $\mu_1 = 0.8$ is obtained using (1.5).

The domain \mathbb{R}^2 is approximated by the square $\Omega = [-L, L]^2$ with $L = 10$, discretized on a uniform grid with mesh size $\Delta x = \Delta y = 0.15$, yielding $M = \left(1 + \frac{2L}{\Delta x}\right)^2 = 17956$ grid points. In this example, we focus on the backward nominal-state input I_{bn} only. See **Fig. 4** for visualization.

7. Conclusion. In this paper, we have investigated the controllability properties of Amari-type neural field equations, with an emphasis on synthesizing piecewise constant-in-time and constant-in-time inputs to steer neural activity from an initial to a desired target state. By constructing explicit constant-in-time input formulas, we extend the theoretical understanding of how sustained inputs can be designed to modulate population activity, opening the door to potential applications in neuroscience, psychophysics, and neurostimulation.

Our numerical illustrations demonstrate the technical feasibility and effectiveness of the proposed feedforward constant-in-time input syntheses (2.27), (3.2), (3.4), and (3.6). In particular, the simulations confirm that these generic syntheses yield significantly smaller endpoint errors and more efficient control efforts compared to naive synthesis (see (6.2)) based on linearizing the dynamics at the initial or target state when they are not equilibria of the drift dynamics.

A natural direction for future work is to integrate experimental data to identify physiologically plausible models and to experimentally validate the proposed synthesis framework—for example, in the context of predicting and mechanistically explaining paradoxical visual illusions as outlined in Section 5.

Appendix A. Proofs of the main results.

In this section, we present the proof of the main results provided in the main text.

A.1. Proof of Theorem 2.4.

Proof. First, we consider the nonlinear map $\Phi : L^p(\mathbb{R}^d) \rightarrow L^p(\mathbb{R}^d)$ defined by

$$(A.1) \quad \Phi(I) = \alpha(1 - e^{-\alpha T})^{-1} \left\{ a_1 - e^{-\alpha T} a_0 - \mu \int_0^T e^{-\alpha(T-t)} \omega * f(a_I(t)) dt \right\}, \quad I \in L^p(\mathbb{R}^d)$$

where $a_I(\cdot) \in C^0([0, T]; L^p(\mathbb{R}^d))$ is the unique solution to (NF) with the input $I \in L^p(\mathbb{R}^d)$, provided by Proposition 2.3. To complete the proof of the theorem, it suffices to show that Φ is $L(T)$ -Lipschitz continuous, where $L(T) > 0$ is defined in (2.5). Let $J \in L^p(\mathbb{R}^d)$, and $a_J(\cdot)$ be the corresponding solution to (NF). One has

$$\Phi(J) - \Phi(I) = \alpha(1 - e^{-\alpha T})^{-1} \mu \int_0^T e^{-\alpha(T-t)} \omega * [f(a_I(t)) - f(a_J(t))] dt$$

which taking the $L^p(\mathbb{R}^d)$ -norm, and Young-convolution inequality yield

$$(A.2) \quad \|\Phi(J) - \Phi(I)\|_p \leq \alpha(1 - e^{-\alpha T})^{-1} \mu \|\omega\|_1 \int_0^T e^{-\alpha(T-t)} \|a_I(t) - a_J(t)\|_p dt.$$

Using (2.1), and Gronwall's lemma, one obtains

$$(A.3) \quad \|a_I(t) - a_J(t)\|_p \leq e^{-\alpha t \left(1 - \frac{\mu}{\mu_0}\right)} \|I - J\|_p \int_0^t e^{\alpha s \left(1 - \frac{\mu}{\mu_0}\right)} ds.$$

Combining (A.2) and (A.3), one deduces

$$(A.4) \quad \|\Phi(J) - \Phi(I)\|_p \leq \alpha^2 \frac{\mu}{\mu_0} \|I - J\|_p (1 - e^{-\alpha T})^{-1} \int_0^T e^{-\alpha(T-t)} e^{-\alpha t \left(1 - \frac{\mu}{\mu_0}\right)} \int_0^t e^{\alpha s \left(1 - \frac{\mu}{\mu_0}\right)} ds dt.$$

Now, if $\mu = \mu_0$, one finds from (A.4) that

$$(A.5) \quad \|\Phi(J) - \Phi(I)\|_p \leq \alpha^2 \frac{\mu}{\mu_0} \|I - J\|_p (1 - e^{-\alpha T})^{-1} \int_0^T e^{-\alpha(T-t)} t dt = \left[\frac{\alpha T}{1 - e^{-\alpha T}} - 1 \right] \|I - J\|_p$$

by using integration by parts of $\alpha \int_0^T e^{-\alpha(T-t)} t dt$. In the case of $\mu \neq \mu_0$, one deduces from (A.4) that

$$(A.6) \quad \|\Phi(J) - \Phi(I)\|_p \leq \frac{1}{r-1} \left(\frac{e^{\alpha r T} - 1}{e^{\alpha T} - 1} - r \right) \|I - J\|_p, \quad r := \frac{\mu}{\mu_0}$$

by performing the integration of

$$\int_0^T e^{-\alpha(T-t)} e^{-\alpha t \left(1 - \frac{\mu}{\mu_0}\right)} \int_0^t e^{\alpha s \left(1 - \frac{\mu}{\mu_0}\right)} ds dt = \frac{1}{\alpha^2(1-r)} \left[(1 - e^{-\alpha T}) + \frac{(1 - e^{\alpha r T})}{r e^{\alpha T}} \right].$$

Inequalities (A.5) and (A.6) show that Φ is $L(T)$ -Lipschitz continuous. Finally, an immediate real analysis shows that $L(T) < 1$ if and only if the conditions in the statement of the theorem are satisfied. \square

A.2. Proof of Theorem 2.9.

Proof. Let $t \in [0, T]$ and set $b : s \in [0, t] \mapsto b(s) \in L^p(\mathbb{R}^d)$ so that $a(s) = V_{T-s}(b(s))$ is the solution of (2.10). Then b is derivable almost everywhere w.r.t. s and it holds

$$(A.7) \quad N(a(s)) + I(s) = \dot{a}(s) = N(a(s)) + DV_{T-s}(b(s))\dot{b}(s)$$

so that using (2.17), we find that b solves the following

$$(A.8) \quad \dot{b}(s) = DU_{T-s}(a(s))I(s), \quad b(0) = U_T(a_0).$$

Integrating (A.8) over $[0, t]$ yields (2.18). Conversely, if (2.18) holds, then $a(0) = a_0$ and $a \in C^0([0, T]; L^p(\mathbb{R}^d))$. Otherwise, there exists (a nondecreasing sequence) $(t_n) \subset [0, T]$, $t_* \in [0, T]$ with $t_n \rightarrow t_*$ and $\varepsilon > 0$ such that $\|U_{T-t_n}(a(t_n)) - U_{T-t_*}(a(t_*))\|_p \geq \varepsilon$. In fact, $a \in C^0([0, T]; L^p(\mathbb{R}^d))$ if and only if $b(t) := U_{T-t}(a(t)) \in C^0([0, T]; L^p(\mathbb{R}^d))$ since U_{T-t} is invertible and C^1 w.r.t. $t \in \mathbb{R}$. However, we have from (2.18) that

$$(A.9) \quad \|U_{T-t_n}(a(t_n)) - U_{T-t_*}(a(t_*))\|_p \leq e^{-\alpha T \left(1 - \frac{\mu}{\mu_0}\right)} e^{\Lambda t_*} \int_{t_n}^{t_*} \|I(s)\|_p ds$$

by using (B.16) with $\gamma(s) = T - s$ and $\beta(s) = a(s)$. It follows that $\|U_{T-t_n}(a(t_n)) - U_{T-t_*}(a(t_*))\|_p \rightarrow 0$ as $n \rightarrow \infty$, which is inconsistent. Letting now

$$(A.10) \quad c(t) := U_T(a_0) + \int_0^t DU_{T-s}(a(s))I(s)ds$$

and deriving (2.18) almost everywhere w.r.t. t yields

$$(A.11) \quad \dot{a}(t) = -\partial_t V_{T-t}(c(t)) + DV_{T-t}(c(t))DU_{T-t}(a(t))I(t) = N(V_{T-t}(c(t))) + I(t) = N(a(t)) + I(t)$$

by $a(t) = V_{T-t}(c(t))$ and $DV_{T-t}(c(t))DU_{T-t}(a(t)) = \text{Id}$. This completes the proof of the theorem. \square

A.3. Proof of Proposition 2.12.

Proof. Theorem 2.9 ensures that the solution $a_\tau(\cdot)$ of (2.10) with the input $I_{sf,\tau}$ defined in (2.20) satisfies

$$(A.12) \quad a_\tau(T) = U_T(a_0) + \int_{T-\tau}^T DU_{T-t}(a_\tau(t))I dt.$$

The function $\phi : t \mapsto \phi(t) = DU_{T-t}(a_\tau(t))I$ belongs to $L^1((0, T); L^p(\mathbb{R}^d))$ by Lemma B.2, and is derivable for almost every $t \in (0, T)$, and

$$(A.13) \quad \dot{\phi}(t) = -DN(U_{T-t}(a_\tau(t)))DU_{T-t}(a_\tau(t))I + \partial DU_{T-t}(a_\tau(t))\dot{a}_\tau(t)I$$

belongs to $L^1((0, T); L^p(\mathbb{R}^d))$ by (2.14) and inequalities (B.16), (A.18) and (A.19) in the appendix. It follows that ϕ is absolutely continuous on $[0, T]$. By evoking (B.1) and (A.16), a similar observation applies to $t \mapsto Z_{t,\tau,T}^n DU_{T-t}(a_\tau(t))I$ for any $n \in \mathbb{N}^*$, where $Z_{t,\tau,T} := DN(U_{T-t}(a_\tau(t)))$. Via a double integration by parts and the fact that $a_\tau(T - \tau) = U_{T-\tau}(a_0)$, one gets

$$\begin{aligned} a_\tau(T) &= U_T(a_0) + \tau DU_\tau(U_{T-\tau}(a_0))I - \frac{\tau^2}{2} DN(U_T(a_0))DU_\tau(U_{T-\tau}(a_0))I + \int_{T-\tau}^T (t-T) \partial DU_{T-t}(a_\tau(t)) \dot{a}_\tau(t) I dt \\ &\quad - \int_{T-\tau}^T \frac{(t-T)^2}{2} \left[\frac{d}{dt} Z_{t,\tau,T} \right] DU_{T-t}(a_\tau(t)) I dt + \int_{T-\tau}^T \frac{(t-T)^2}{2} Z_{t,\tau,T} \partial DU_{T-t}(a_\tau(s)) \dot{a}_\tau(t) I dt \\ (A.14) \quad &+ \int_{T-\tau}^T \frac{(t-T)^2}{2} Z_{t,\tau,T}^2 DU_{T-t}(a_\tau(t)) I dt \end{aligned}$$

from which one performs another integration by parts on the last integral in (A.14) and so on to obtain (F1) and (2.21). Here $\partial DU_{T-t}(a_\tau(t)) \dot{a}_\tau(t) I$ is the Gâteaux derivative of DU_{T-t} at $a_\tau(t)$ in the direction $\dot{a}_\tau(t)$, and applied to I . Finally, the series (F1) and (2.21) are well-defined by Lemma A.1. \square

Finally, the following result shows that the series in Proposition 2.12 are well-defined.

LEMMA A.1. *The series in (F1) is well-defined in $\mathcal{L}(L^p(\mathbb{R}^d))$ for every $p \in (1, \infty]$, and the series in (2.21) are well-defined in $\mathcal{L}(L^p(\mathbb{R}^d))$ for every $p \in [2, \infty]$. Moreover, it holds*

$$(A.15) \quad \|\varphi_{\tau,T}(I)\|_{\mathcal{L}(L^p(\mathbb{R}^d))} \leq C\tau^3$$

for some $C := C(\tau, T, \alpha, \mu, \mu_0, \|\omega\|_q, \|f''\|_\infty, \|a_0\|_p, \|I\|_p) > 0$.

Proof. First of all, the series in (F1) is well-defined in $\mathcal{L}(L^p(\mathbb{R}^d))$ by invoking the exponential operator (1.1). On the other hand, one has for every $n \geq 1$

$$(A.16) \quad \frac{d}{dt} Z_{t,\tau,T}^n = \sum_{k=1}^n Z_{t,\tau,T}^{k-1} \dot{Z}_{t,\tau,T} Z_{t,\tau,T}^{n-k}$$

where $\dot{Z}_{t,\tau,T} = -\partial DN(U_t(a_\tau(T-t)))DU_t(a_\tau(T-t))I$ using (2.18). One deduces from (A.16) and (B.1), and by applying (B.16) with $\gamma(t) = t$ and $\beta(t) = a_\tau(T-t)$ that for every $b \in L^p(\mathbb{R}^d)$,

$$(A.17) \quad \|\kappa_{\tau,T}(I)\|_{\mathcal{L}(L^p(\mathbb{R}^d))} \leq \Lambda_1 \|I\|_p \max\left(1, e^{-2\alpha\tau(1-\frac{\mu}{\mu_0})}\right) \sum_{n=1}^{\infty} \int_0^\tau \frac{t^{n+1} n \Lambda^n}{(n+1)!} dt \leq C_0 \tau^3$$

for some $C_0 := C_0(\tau, \alpha, \mu, \mu_0, \|a_0\|_p, \|I\|_p, \|\omega\|_q, \|f''\|_\infty) > 0$. Now, if $I \in L^p(\mathbb{R}^d)$ is constant in time, $\dot{a}_\tau(T-t) = -N(a_\tau(T-t)) - I$ satisfies

$$(A.18) \quad \|\dot{a}_\tau(T-t)\|_p \leq \Lambda e^{-\alpha(T-t)(1-\frac{\mu}{\mu_0})} \|a_0\|_p + \Lambda(T-t) \max(1, e^{-\alpha(T-t)(1-\frac{\mu}{\mu_0})}) \|I\|_p + \|I\|_p$$

by (2.2). On the other hand, by applying (B.17) with $\gamma(t) = t$, $\beta(t) = a_\tau(T-t)$ and $h = \dot{a}_\tau(T-t)$, one gets,

$$(A.19) \quad \|\partial DU_t(a_\tau(T-t)) \dot{a}_\tau(T-t)\|_{\mathcal{L}(L^p(\mathbb{R}^d))} \leq \Lambda_1 t e^{-\alpha t(1-\frac{\mu}{\mu_0})} \|\dot{a}_\tau(T-t)\|_p \leq C_1 t$$

for some $C_1 := C_1(\tau, T, \alpha, \mu, \mu_0, \|a_0\|_p, \|I\|_p, \|\omega\|_q, \|f''\|_\infty)$ using (A.18) and $0 \leq t \leq \tau \leq T$. It follows from $\|Z_{t,\tau,T}\|_{\mathcal{L}(L^p(\mathbb{R}^d))} \leq \Lambda$ and (A.19) that

$$(A.20) \quad \|\chi_{\tau,T}(I)\|_{\mathcal{L}(L^p(\mathbb{R}^d))} \leq C_1 \sum_{n=1}^{\infty} \int_0^\tau \frac{t^{n+1} \Lambda^{n-1}}{(n+1)!} dt \leq C_1 e^{\Lambda\tau} \tau^3.$$

Combining (A.17) and (A.20) yields (A.15). \square

A.4. Proof of Theorem 2.16.

Proof. Let us show that $a_\tau(T) = a_1$ is equivalent to (2.23). Using (F1) and left multiplying $a_\tau(T) = a_1$ by $DN(U_T(a_0))$ yields

$$(A.21) \quad DN(U_T(a_0))(a_1 - U_T(a_0)) = -\mathcal{D}_T(a_0)\varphi_{\tau,T}(I)I + \left(\text{Id} - e^{-\tau\mathcal{D}_T(a_0)}\right) DU_\tau(U_{T-\tau}(a_0))I$$

where $\mathcal{D}_T(a_0) := DN(U_T(a_0))$. Since $[DU_\tau(U_{T-\tau}(a_0))]^{-1} = DV_\tau(U_T(a_0))$, one finds from (A.21) that

$$DV_\tau(U_T(a_0)) \left(\text{Id} - e^{-\tau\mathcal{D}_T(a_0)}\right)^{-1} \mathcal{D}_T(a_0)(a_1 - U_T(a_0)) = I - DV_\tau(U_T(a_0)) \left(\text{Id} - e^{-\tau\mathcal{D}_T(a_0)}\right)^{-1} \mathcal{D}_T(a_0)\varphi_{\tau,T}(I)I$$

which implies that $I \in L^p(\mathbb{R}^d)$ solves

$$(A.22) \quad [\text{Id} - \mathcal{A}_{\tau,T}(a_0)\varphi_{\tau,T}(I)]I = \mathcal{A}_{\tau,T}(a_0)(a_1 - U_T(a_0))$$

where $\mathcal{A}_{\tau,T}(a_0)$ is defined by (2.24). This completes the proof of the sufficient part. Assume now that $I \in L^p(\mathbb{R}^d)$ satisfies (2.23). It follows that

$$(A.23) \quad DN(U_T(a_0))(a_1 - U_T(a_0)) = \left(e^{-\tau DN(U_T(a_0))} - \text{Id}\right) DU_\tau(U_{T-\tau}(a_0))I - DN(U_T(a_0))\varphi_{\tau,T}(I)I.$$

From (F1), one finds

$$(A.24) \quad DN(U_T(a_0))(a_\tau(T) - a_0) = \left(e^{-\tau DN(U_T(a_0))} - \text{Id}\right) DU_\tau(U_{T-\tau}(a_0))I - DN(U_T(a_0))\varphi_{\tau,T}(I)I.$$

Identifying (A.23) with (A.24), one deduces that $DN(U_T(a_0))(a_\tau(T) - a_1) = 0$ so that $a_\tau(T) = a_1$ since $DN(U_T(a_0))$ is invertible. This completes the proof of the theorem. \square

A.5. Proof of Proposition 2.18.

Proof. Let $I \in L^p(\mathbb{R}^d)$ and $I_{sf,\tau}(\cdot)$ be the step function defined by (2.20). Then, the corresponding solution $a_\tau(\cdot)$ to (2.10) is given by

$$a_\tau(t) = U_t(a_0), \quad 0 \leq t \leq T - \tau, \quad T \geq \tau > 0,$$

$$a_\tau(t) = U_{t-T}(U_T(a_0) + b_\tau(t)), \quad b_\tau(t) := \int_{T-\tau}^t DU_{T-s}(a(s)) ds I, \quad T - \tau < t \leq T, \quad T \geq \tau > 0$$

by Theorem 2.9. Applying (B.16) with $\gamma(t) = T - t$ and $\beta(t) = a(t)$, one finds

$$\|b_\tau(t)\|_p \leq \|I\|_p e^{-\alpha T(1 - \frac{\mu}{\mu_0})} \int_{T-\tau}^t e^{\alpha s(1 + \frac{\mu}{\mu_0})} ds \leq \|I\|_p e^{-\alpha T(1 - \frac{\mu}{\mu_0})} e^{\alpha t(1 + \frac{\mu}{\mu_0})} \tau$$

so that $b_\tau(t) = \mathcal{O}(\tau)$ as $\tau \rightarrow 0$. It follows that

$$a_\tau(t) = U_t(a_0) + \mathcal{O}(\tau) \quad \text{as } \tau \rightarrow 0, \quad \forall t \in [0, T].$$

Therefore, one deduces the following expansions, which hold for every $t \in [0, T]$:

$$Z_{t,\tau,T} := DN(U_t(a_\tau(T-t))) \underset{\tau \sim 0}{=} \Phi_T(a_0) + \mathcal{O}(\tau), \quad Q_{t,\tau,T} := DU_t(a_\tau(T-t)) \underset{\tau \sim 0}{=} DU_t(U_{T-t}(a_0)) + \mathcal{O}(\tau),$$

$$P_{t,\tau,T} := \partial DU_t(a_\tau(T-t)) \dot{a}_\tau(T-t) \underset{\tau \sim 0}{=} \partial DU_t(U_{T-t}(a_0)) N(U_{T-t}(a_0)) + \mathcal{O}(\tau)$$

where $\Phi_T(a_0) := DN(U_T(a_0))$. Thus, from (2.21), one gets

$$(A.25) \quad \kappa_{\tau,T}(I) \underset{\tau \sim 0}{=} \mathcal{O}(\tau^4), \quad \chi_{\tau,T}(I) \underset{\tau \sim 0}{=} \chi_{\tau,T}(a_0) + \mathcal{O}(\tau^4)$$

where, using (B.33), one has

$$\chi_{\tau,T}(a_0) := \sum_{n=1}^{\infty} \int_0^{\tau} \frac{(-t)^n \Phi_T(a_0)^{n-1}}{n!} [\Phi_T(a_0) DU_t(U_{T-t}(a_0)) - DU_t(U_{T-t}(a_0)) DN(U_{T-t}(a_0))] dt.$$

Via integration by parts, one finds

$$\begin{aligned} \chi_{\tau,T}(a_0) &= \int_0^{\tau} [e^{-t\Phi_T(a_0)} - \text{Id}] DU_t(U_{T-t}(a_0)) dt - \sum_{n=1}^{\infty} \int_0^{\tau} \frac{(-t)^n \Phi_T(a_0)}{n!} \left[\frac{d}{dt} DU_t(U_{T-t}(a_0)) \right] dt \\ &= [\text{Id} - e^{-\tau\Phi_T(a_0)}] \Phi_T(a_0)^{-1} DU_{\tau}(U_{T-\tau}(a_0)) + [e^{\tau\Phi_T(a_0)} - \text{Id}] \Phi_T(a_0)^{-1} \\ &\quad - \underbrace{\sum_{n=1}^{\infty} \int_0^{\tau} \frac{(t-\tau)^{n+1} DU_t(U_{T-t}(a_0))}{(n+1)!} \left[\frac{d}{dt} Z_{t,T}^n \right] dt}_{\Lambda_{\tau,T}(a_0)}. \end{aligned} \tag{A.26}$$

where $Z_{t,T} := DN(U_{T-t}(a_0))$. Therefore, using an identity such as (A.16), one deduces that

$$\Lambda_{\tau,T}(a_0) \leq C\tau^3, \quad \text{for some } C := C(\tau, T, \alpha, \mu, \|f''\|_{\infty}, \|\omega\|_q, \|a_0\|_p) > 0$$

by (B.1), (2.14) and (B.16). It follows from (A.25) and (A.26) that $\varphi_{\tau,T}(I) := \kappa_{\tau,T}(I) + \chi_{\tau,T}(I)$ expands as in (2.25). Finally, the expansion (2.26) follows from (2.25), (2.24), and the fact that $[e^{\tau\Phi_T(a_0)} - \text{Id}]^{-1} \underset{\tau \sim 0}{=} \mathcal{O}(\tau^{-1})$ since $\Phi_T(a_0)$ is uniformly bounded with respect to T and a_0 . \square

Appendix B. Some useful properties of the drift and its associated flow operators.

In the following, we prove some valuable properties of the nonlinear operator N defined in (2.11).

PROPOSITION B.1. *The following holds.*

1. *If $2 \leq p \leq \infty$, then the Fréchet derivative DN is Gâteaux differentiable at any $u \in L^p(\mathbb{R}^d)$, and for every $h \in L^p(\mathbb{R}^d)$, $\partial DN(u)h \in \mathcal{L}(L^p(\mathbb{R}^d))$ satisfies*

$$\begin{aligned} \partial DN(u)hv &= \mu\omega * [f''(u)hv], \quad \forall v \in L^p(\mathbb{R}^d) \\ \|\partial DN(u)h\|_{\mathcal{L}(L^p(\mathbb{R}^d))} &\leq \mu \|f''\|_{\infty} \|\omega\|_q \|h\|_p. \end{aligned} \tag{B.1}$$

2. *Assume that f is third times derivable and the third derivative $f^{(3)}$ is bounded. If $2 < p \leq \infty$, then $N \in C^2(L^p(\mathbb{R}^d); L^p(\mathbb{R}^d))$ and its second differential at $u \in L^p(\mathbb{R}^d)$ satisfies*

$$\begin{aligned} D^2N(u)hv &= \partial DN(u)hv = \mu\omega * [f''(u)hv], \quad \forall (h, v) \in L^p(\mathbb{R}^d) \times L^p(\mathbb{R}^d) \\ \|D^2N(u)\|_{\mathcal{L}(L^p(\mathbb{R}^d)^2; L^p(\mathbb{R}^d))} &\leq \mu \|f''\|_{\infty} \|\omega\|_q. \end{aligned} \tag{B.2}$$

Here q is the conjugate to p .

Proof. It is a consequence of [50, Lemma B. 8] that under Assumption 1.2, $N \in C^1(L^p(\mathbb{R}^d); L^p(\mathbb{R}^d))$ for every $1 < p \leq \infty$. It is straightforward to show that the Gâteaux derivative of $M := DN$ at $u \in L^p(\mathbb{R}^d)$ in the direction $h \in L^p(\mathbb{R}^d)$ applied to $v \in L^p(\mathbb{R}^d)$ is given by

$$\partial M(u)hv(x) = \mu(\omega * [f''(u)hv])(x) = \mu \int_{\mathbb{R}^d} \omega(x-y) f''(u(y)) h(y) v(y) dy, \quad \forall x \in \mathbb{R}^d. \tag{B.3}$$

One has that $\partial M(u)hv$ is bilinear with respect to h and v . When $p = \infty$, the inequality in (B.1) is an immediate consequence of the Young-convolution inequality applied to (B.3). In the case of $2 \leq p < \infty$, one has

$$\|\partial M(u)hv\|_p^p = \mu^p \int_{\mathbb{R}^d} |\Gamma(x)|^p dx, \quad \Gamma(x) := \int_{\mathbb{R}^d} \omega(x-y) f''(u(y)) h(y) v(y) dy. \tag{B.4}$$

By Hölder inequality, and the generalized Jensen inequality, we find⁶

$$(B.5) \quad |\Gamma(x)|^p \leq \|f''\|_\infty^p \|\omega\|_q^p \left(\int_{\mathbb{R}^d} |h(y)|^p \frac{|\omega(x-y)|^q}{\|\omega\|_q^q} dy \right) \|v\|_p^p$$

whenever $p/q \geq 1$, i.e. $2 \leq p < \infty$. Integrating (B.5) over \mathbb{R}^d , using Fubini theorem, one gets

$$(B.6) \quad \Gamma^p \leq \|f''\|_\infty^p \|\omega\|_q^p \|h\|_p^p \|v\|_p^p.$$

Therefore, (B.1) follows immediately by (B.3), (B.4) and (B.6).

To prove that M is differentiable (that is, N is twice differentiable)–in the Fréchet sense–when f is thirdly derivable and $f^{(3)}$ is bounded, it suffices to prove that the Gâteaux derivative

$$(B.7) \quad \partial M : L^p(\mathbb{R}^d) \longrightarrow \mathcal{L}(L^p(\mathbb{R}^d)^2; L^p(\mathbb{R}^d)), \quad u \longmapsto \partial M(u)$$

is continuous. To this end, let $(u_n) \subset L^p(\mathbb{R}^d)$ be a real sequence converging in the L^p -norm to $u \in L^p(\mathbb{R}^d)$. We want to prove that $\partial M(u_n)$ converges to $\partial M(u)$ in $\mathcal{L}(L^p(\mathbb{R}^d)^2; L^p(\mathbb{R}^d))$. Let $(h, v) \in L^p(\mathbb{R}^d)^2$ and set

$$(B.8) \quad \Gamma_n : x \in \mathbb{R}^d \longmapsto \Gamma_n(x) = \int_{\mathbb{R}^d} \omega(x-y) [f''(u_n(y)) - f''(u(y))] h(y) v(y) dy.$$

Since f'' is $\|f^{(3)}\|_\infty$ -Lipschitz continuous, one immediately gets that

$$\|\Gamma_n\|_\infty \leq \|f^{(3)}\|_\infty \|\omega\|_1 \|u_n - u\|_\infty \|h\|_\infty \|v\|_\infty$$

by Young's convolution inequality. It follows that

$$(B.9) \quad \|\partial M(u_n) - \partial M(u)\|_{\mathcal{L}(L^\infty(\mathbb{R}^d)^2; L^\infty(\mathbb{R}^d))} \leq \mu \|f^{(3)}\|_\infty \|\omega\|_1 \|u_n - u\|_\infty \xrightarrow{n \rightarrow \infty} 0.$$

Let us turn to an argument for $2 < p < \infty$. Since (u_n) tends in the L^p -norm to $u \in L^p(\mathbb{R}^d)$, for every $\varepsilon > 0$, there exists $N \in \mathbb{N}$ such that for any $n \geq N$ it holds $\|u_n - u\|_p \leq \varepsilon$. We fix the previously defined $\varepsilon > 0$ and N in the following, and we consider $E_n := \{y \in \mathbb{R}^d \mid |u_n(y) - u(y)| > \sqrt{\varepsilon}\}$. One has for every $x \in \mathbb{R}^d$,

$$(B.10) \quad \Gamma_n(x) = \underbrace{\int_{\mathbb{R}^d \setminus E_n} \omega(x-y) [f''(u_n(y)) - f''(u(y))] h(y) v(y) dy}_{\Lambda_1(x)} + \underbrace{\int_{E_n} \omega(x-y) [f''(u_n(y)) - f''(u(y))] h(y) v(y) dy}_{\Lambda_2(x)}.$$

By Chebyshev's inequality, it holds that

$$(B.11) \quad |E_n| \leq \frac{\|u_n - u\|_p^p}{\varepsilon^{\frac{p}{2}}} \leq \varepsilon^{\frac{p}{2}}$$

where $|E_n|$ denotes the Lebesgue measure of the measurable set $E_n \subset \mathbb{R}^d$.

On one hand, since f'' is $\|f^{(3)}\|_\infty$ -Lipschitz continuous, one has by arguing as in the proof of (B.6),

$$(B.12) \quad \|\Lambda_1\|_p \leq \|f^{(3)}\|_\infty \|\omega\|_q \sqrt{\varepsilon} \|h\|_p \|v\|_p.$$

On the other hand, using Hölder's inequality and the fact that f'' is bounded, one finds

$$(B.13) \quad |\Lambda_2(x)|^p \leq 2^p \|f''\|_\infty^p |E_n|^{\frac{p}{q}-1} \int_{E_n} |\omega(x-y)|^p |h(y)|^p dy \|v\|_p^p, \quad \forall x \in \mathbb{R}^d$$

⁶Remembering that $\omega \in \mathcal{S}(\mathbb{R}^d)$ or that $\omega \in L^1(\mathbb{R}^d) \cap L^p(\mathbb{R}^d) \cap L^q(\mathbb{R}^d)$.

by generalized Jensen's inequality. Integrating the above inequality with variable x over \mathbb{R}^d , we find,

$$(B.14) \quad \|\Lambda_2\|_p := \left\{ \int_{\mathbb{R}^d} |\Lambda_2(x)|^p dx \right\}^{\frac{1}{p}} \leq 2\|f''\|_\infty |E_n|^{\frac{1}{q} - \frac{1}{p}} \|\omega\|_p \|h\|_p \|v\|_p \leq 2\|f''\|_\infty \|\omega\|_p \|h\|_p \|v\|_p (\sqrt{\varepsilon})^{p-2}$$

Fubini's theorem, where the last inequality is obtained owing to (B.11) and $p/q = p - 1$. Taking now the $L^p(\mathbb{R}^d)$ -norm of both sides of (B.10), applying Minkowski's inequality and using (B.12) and (B.14), one gets

$$(B.15) \quad \|\partial M(u_n) - \partial M(u)\|_{\mathcal{L}(L^p(\mathbb{R}^d)^2; L^p(\mathbb{R}^d))} \leq \mu(\|f^{(3)}\|_\infty \|\omega\|_q + 2\|f''\|_\infty \|\omega\|_p) \max(\sqrt{\varepsilon}, (\sqrt{\varepsilon})^{p-2}).$$

It follows that the operator ∂M defined in (B.7) is continuous, and (B.2) follows immediately. \square

The following lemma is more general than [50, Lemma B. 10] given that the operator norm of $DU_t(u)$ does not systematically grow with $t \geq 0$ as one might think by examining [50, Lemma B. 10].

LEMMA B.2. *Let $p \in (1, \infty]$, $\beta \in C^0(\mathbb{R}_+; L^p(\mathbb{R}^d))$, and $\gamma \in C^1(\mathbb{R}_+; \mathbb{R})$ with $\gamma(0) \geq 0$. Then, for every $t \geq 0$, it holds*

$$(B.16) \quad \|DU_{\gamma(t)}(\beta(t))\|_{\mathcal{L}(L^p(\mathbb{R}^d))} \leq e^{-\alpha\gamma(0)} \left(1 - \frac{\mu}{\mu_0}\right) e^{-\alpha \int_0^t \dot{\gamma}(\tau) d\tau} e^{\alpha \frac{\mu}{\mu_0} \int_0^t |\dot{\gamma}(\tau)| d\tau}.$$

If $p \in [2, \infty]$, then for all $h \in L^p(\mathbb{R}^d)$ and every $t \geq 0$, it holds

$$(B.17) \quad \|\partial DU_{\gamma(t)}(\beta(t))h\|_{\mathcal{L}(L^p(\mathbb{R}^d))} \leq \Lambda_1 e^{-\alpha \int_0^t \dot{\gamma}(\tau) d\tau} e^{\alpha \frac{\mu}{\mu_0} \int_0^t |\dot{\gamma}(\tau)| d\tau} e^{-\alpha \left(1 - \frac{\mu}{\mu_0}\right) \gamma(0)} (\|\dot{\gamma}\|_\infty t + \gamma(0)) \|h\|_p$$

where $\|\dot{\gamma}\|_\infty := \max_{0 \leq s \leq t} |\dot{\gamma}(s)|$, $\Lambda_1 := \mu\|f''\|_\infty \|\omega\|_q$ and $\partial DU_{\gamma(t)}$ is the Gâteaux derivative of $DU_{\gamma(t)}$.

In the specific case of $p = 2$, one can sharpen (B.16) and (B.17) by replacing μ_0 by μ_1 .

Proof. Let $v, h \in L^p(\mathbb{R}^d)$ and $\gamma \in C^1(\mathbb{R}_+, \mathbb{R})$ such that $\gamma(0) \geq 0$. It follows from (2.16) that

$$(B.18) \quad \dot{y}(t) = -\alpha\dot{\gamma}(t)y(t) + \mu\dot{\gamma}(t)\omega * [f'(U_{\gamma(t)}(v))y(t)], \quad y(t) := DU_{\gamma(t)}(v)h, \quad \forall t \geq 0$$

which yields the following integral representation

$$(B.19) \quad y(t) = e^{-\alpha \int_0^t \dot{\gamma}(\tau) d\tau} y(0) + \mu \int_0^t \dot{\gamma}(s) e^{-\alpha \int_0^t \dot{\gamma}(\tau) d\tau} e^{\alpha \int_0^s \dot{\gamma}(\tau) d\tau} \omega * [f'(U_{\gamma(s)}(v))y(s)] ds.$$

Taking the $L^\infty(\mathbb{R}^d)$ -norm yields

$$(B.20) \quad \|y(t)\|_\infty \leq e^{-\alpha \int_0^t \dot{\gamma}(\tau) d\tau} e^{\alpha \frac{\mu}{\mu_0} \int_0^t |\dot{\gamma}(\tau)| d\tau} e^{-\alpha \left(1 - \frac{\mu}{\mu_0}\right) \gamma(0)} \|h\|_\infty.$$

Let $\beta \in C^0(\mathbb{R}_+; L^\infty(\mathbb{R}^d))$, then for a fixed $t \geq 0$, the map $s \mapsto DU_{\gamma(t)}(\beta(s))$ is continuous by composition, and using (B.20), we find

$$(B.21) \quad \|DU_{\gamma(t)}(\beta(s))\|_{\mathcal{L}(L^\infty(\mathbb{R}^d))} \leq e^{-\alpha \int_0^t \dot{\gamma}(\tau) d\tau} e^{\alpha \frac{\mu}{\mu_0} \int_0^t |\dot{\gamma}(\tau)| d\tau} e^{-\alpha \left(1 - \frac{\mu}{\mu_0}\right) \gamma(0)}, \quad \forall s \in [0, t]$$

which proves (B.16) by continuity and taking the lim sup as $s \rightarrow t$.

If $1 < p < \infty$, one uses the last paragraph of Notation 1.1 as follows. One has from (B.18),

$$(B.22) \quad \frac{1}{2} \frac{d}{dt} \|y(t)\|_p^2 = D\varphi(y(t))\dot{y}(t) = \langle y(t)^*, \dot{y}(t) \rangle_{L^q, L^p} \leq (-\alpha\dot{\gamma}(t) + \mu\|\omega\|_1 |\dot{\gamma}(t)|) \|y(t)\|_p^2$$

by Hölder and Young's convolution inequalities. It follows that

$$(B.23) \quad \|y(t)\|_p \leq e^{-\alpha \int_0^t \dot{\gamma}(\tau) d\tau} e^{\alpha \frac{\mu}{\mu_0} \int_0^t |\dot{\gamma}(\tau)| d\tau} \|y(0)\|_p, \quad \forall t \geq 0$$

by Gronwall's lemma. One concludes the proof by arguing as in the case of $p = \infty$.

Beside the above analysis that contains the case of $p = 2$, by taking advantage of the Fourier transform properties' in $L^2(\mathbb{R}^d)$, one gets

$$(B.24) \quad \frac{1}{2} \frac{d}{dt} \|y(s)\|_2^2 = \langle y(t), DN(U_{\gamma(t)}(v))y(t) \rangle_{L^2} \leq -\alpha \dot{\gamma}(t) \|y(t)\|_2^2 + \mu |\dot{\gamma}(t)| \|\widehat{\omega}\|_\infty \|y(t)\|_2^2.$$

by Parseval's identity and Plancherel's theorem. Inequalities (B.16) follow by arguing as previously.

Now, letting $y(t)$ as previously, $z(t) := \partial DU_{\gamma(t)}(v)h$, and using (2.16), we find

$$(B.25) \quad \dot{z}(t) = -\alpha \dot{\gamma}(t) z(t) + \mu \dot{\gamma}(t) \omega * [f'(U_{\gamma(t)}(v))z(t)] + \dot{\gamma}(t) \partial DN(U_{\gamma(t)}(v))y(t), \quad z(0) = \partial DU_{\gamma(0)}(v)h.$$

Taking the $L^p(\mathbb{R}^d)$ -norm (immediate in the case of $p = \infty$, while for $2 \leq p < \infty$, one can argue as previously) and using (B.1) and (B.20), we find by Gronwall's lemma,

$$(B.26) \quad \|\partial DU_{\gamma(t)}(v)h\|_{\mathcal{L}(L^p(\mathbb{R}^d))} \leq \Lambda_1 e^{-\alpha \int_0^t \dot{\gamma}(\tau) d\tau} e^{\alpha \frac{\mu}{\mu_0} \int_0^t |\dot{\gamma}(\tau)| d\tau} e^{-\alpha \left(1 - \frac{\mu}{\mu_0}\right) \gamma(0)} (\|\dot{\gamma}\|_\infty t + \gamma(0)) \|h\|_p.$$

One completes the proof of (B.17) by arguing as previously. In the specific case of $p = 2$, one proves (B.17) by arguing as in the proof of (B.16) above. \square

We also have the following key results.

LEMMA B.3. *Let $p \in (1, \infty]$, $a \in L^p(\mathbb{R}^d)$, and let $s, t \in \mathbb{R}_+$. Let $\Phi_t(a) := DN(U_t(a))$ where DN is the differential of N , and U_t its flow at t . Then, it holds*

$$(B.27) \quad \|e^{t\Phi_s(a)}\|_{\mathcal{L}(L^p(\mathbb{R}^d))} \begin{cases} \leq e^{-\alpha \left(1 - \frac{\mu}{\mu_0}\right) t} & \text{if } 1 < p \leq \infty \\ \leq e^{-\alpha \left(1 - \frac{\mu}{\mu_1}\right) t} & \text{if } p = 2. \end{cases}$$

Proof. Fix $s \in \mathbb{R}_+$, let $u \in L^p(\mathbb{R}^d)$, and define $c(t) = e^{t\Phi_s(a)}u$, for $t \in \mathbb{R}_+$. Then, $c \in C^1(\mathbb{R}_+; L^p(\mathbb{R}^d))$, $c(0) = u$, and it holds

$$(B.28) \quad \dot{c}(t) = \Phi_s(a)c(t) = -\alpha c(t) + \mu \omega * [f'(U_s(a))c(t)].$$

Assume that $p = \infty$, and represent (B.28) under its integral form by

$$(B.29) \quad c(t) = e^{-\alpha t} u + \mu \int_0^t e^{-\alpha(t-\tau)} \omega * [f'(U_s(a))c(\tau)] d\tau.$$

Since $\|f'(U_s(a))\|_\infty \leq 1$, taking the $L^\infty(\mathbb{R}^d)$ -norm of (B.29), and using by Gronwall's lemma, we find

$$(B.30) \quad \|e^{t\Phi_s(a)}u\|_\infty \leq e^{-\alpha \left(1 - \frac{\mu}{\mu_0}\right) t} \|u\|_\infty \quad \forall s, t \in \mathbb{R}_+.$$

In the cases of $1 < p < \infty$, we introduce for every $t \in \mathbb{R}_+$, $g(t) = \|c(t)\|_p^2$ where c is defined as previously. Therefore, $g \in C^1(\mathbb{R}_+)$, $g(0) = \|u\|_p^2$, and owing to the last paragraph of Notation 1.1, we get from (B.28) that

$$(B.31) \quad \frac{1}{2} \dot{g}(t) = \langle c(t)^*, \dot{c}(t) \rangle_{L^q, L^p} \leq -\alpha \|c(t)\|_p^2 + \mu \|c(t)\|_p^{2-p} \|c(t)\|_p^{p-1} \|\omega\|_1 \|c(t)\|_p = -(\alpha - \mu \|\omega\|_1) g(t)$$

by Hölder and Young's convolution inequalities. Gronwall's inequality to (B.31) yields the desired result. Finally, for $p = 2$, one uses a Fourier transform argument as in the proof of Lemma B.2 to replace (B.31) by

$$(B.32) \quad \dot{g}(t) \leq -2(\alpha - \mu \|\widehat{\omega}\|_\infty) g(t).$$

This completes the proof of the lemma. \square

The proof of the following can be done by mimicking its finite-dimension counterpart [47, Lemma C.4].

LEMMA B.4. *Let $p \in [2, \infty]$, $a \in L^p(\mathbb{R}^d)$, and let $T > 0$, $t \in [0, T]$. The following identity holds*

$$(B.33) \quad DN(U_T(a)) DU_t(U_{T-t}(a)) = DU_t(U_{T-t}(a)) DN(U_{T-t}(a)) + \partial DU_t(U_{T-t}(a)) N(U_{T-t}(a))$$

where ∂DU_{T-t} denotes the Gâteaux derivative of the Fréchet derivative DU_t at $U_{T-t}(a)$.

In particular, when $t = T$, we obtain

$$(B.34) \quad DN(U_T(a)) = DU_T(a) DN(a) DU_T(a)^{-1} + \partial DU_T(a) N(a) DU_T(a)^{-1}.$$

REFERENCES

- [1] A. AGRACHEV AND R. V. GAMKRELIDZE, *The exponential representation of flows and the chronological calculus*, Mathematics of the USSR-Sbornik, 35 (1979), p. 727.
- [2] S.-I. AMARI, *Dynamics of pattern formation in lateral-inhibition type neural fields*, Biological cybernetics, 27 (1977), pp. 77–87.
- [3] A. M. ANNABI, J.-B. POMET, D. PRANDI, AND L. SACCHELLI, *Activity estimation via distributed measurements in an orientation sensitive neural fields model of the visual cortex*, Mathematics of Control, Signals, and Systems, (2025), pp. 1–31.
- [4] A. ASADI, M. MADADI ASL, A. VALIZADEH, AND M. PERC, *Dynamics of parkinsonian oscillations mediated by transmission delays in a mean-field model of the basal ganglia*, Frontiers in Cellular Neuroscience, 18 (2024), p. 1344149.
- [5] T. O. BERGMANN, S. GROPPA, M. SEEGER, M. MÖLLE, L. MARSHALL, AND H. R. SIEBNER, *Acute changes in motor cortical excitability during slow oscillatory and constant anodal transcranial direct current stimulation*, Journal of neurophysiology, 102 (2009), pp. 2303–2311.
- [6] M. BERTALMIÓ, L. CALATRONI, V. FRANCESCHI, B. FRANCESCHIELLO, A. GOMEZ VILLA, AND D. PRANDI, *Visual illusions via neural dynamics: Wilson-cowan-type models and the efficient representation principle*, Journal of neurophysiology, 123 (2020), pp. 1606–1618.
- [7] J. BEZANSON, A. EDELMAN, S. KARPINSKI, AND V. B. SHAH, *Julia: A fresh approach to numerical computing*, SIAM review, 59 (2017), pp. 65–98.
- [8] V. A. BILLOCK AND B. H. TSOU, *Neural interactions between flicker-induced self-organized visual hallucinations and physical stimuli*, Proceedings of the National Academy of Sciences, 104 (2007), pp. 8490–8495.
- [9] V. A. BILLOCK AND B. H. TSOU, *Elementary visual hallucinations and their relationships to neural pattern-forming mechanisms.*, Psychological bulletin, 138 (2012), p. 744.
- [10] M. BOLELLI AND D. PRANDI, *Neural field equations with time-periodic external inputs and some applications to visual processing*, J Math Imaging Vis, 67 (2025), p. 47, <https://doi.org/10.1007/s10851-025-01257-7>.
- [11] P. C. BRESSLOFF, *Spatiotemporal dynamics of continuum neural fields*, Journal of Physics A: Mathematical and Theoretical, 45 (2011), p. 033001.
- [12] P. C. BRESSLOFF, J. D. COWAN, M. GOLUBITSKY, P. J. THOMAS, AND M. C. WIENER, *Geometric visual hallucinations, euclidean symmetry and the functional architecture of striate cortex*, Philosophical Transactions of the Royal Society of London. Series B: Biological Sciences, 356 (2001), pp. 299–330.
- [13] L. BRIVADIS, A. CHAILLET, AND J. AURIOL, *Adaptive observer and control of spatiotemporal delayed neural fields*, Systems & Control Letters, 186 (2024), p. 105777.
- [14] L. BRIVADIS, C. TAMEKUE, A. CHAILLET, AND J. AURIOL, *Existence of an equilibrium for delayed neural fields under output proportional feedback*, Automatica, 151 (2023), p. 110909.
- [15] A. CHAILLET, G. I. DETORAKIS, S. PALFI, AND S. SENOVA, *Robust stabilization of delayed neural fields with partial measurement and actuation*, Automatica, 83 (2017), pp. 262–274.
- [16] P. G. CIARLET, *Linear and Nonlinear Functional Analysis with Applications*, Society for Industrial and Applied Mathematics (SIAM), Philadelphia, PA, 2013.
- [17] B. J. COOK, A. D. PETERSON, W. WOLDMAN, AND J. R. TERRY, *Neural field models: A mathematical overview and unifying framework*, Mathematical Neuroscience and Applications, 2 (2022).
- [18] S. COOMBES, *Waves, bumps, and patterns in neural field theories*, Biological cybernetics, 93 (2005), pp. 91–108.
- [19] S. COOMBES, *Next generation neural population models*, Frontiers in Applied Mathematics and Statistics, 9 (2023), p. 1128224.
- [20] S. COOMBES, P. BEIM GRABEN, AND R. POTTHAST, *Tutorial on Neural Field Theory*, Springer Berlin Heidelberg, Berlin, Heidelberg, 2014, pp. 1–43, https://doi.org/10.1007/978-3-642-54593-1_1.
- [21] S. COOMBES AND C. LAING, *Delays in activity-based neural networks*, Philosophical Transactions of the Royal Society A: Mathematical, Physical and Engineering Sciences, 367 (2009), pp. 1117–1129.
- [22] R. CURTU AND B. ERMENTROUT, *Pattern formation in a network of excitatory and inhibitory cells with adaptation*, SIAM Journal on Applied Dynamical Systems, 3 (2004), pp. 191–231.
- [23] B. ERMENTROUT, *Neural networks as spatio-temporal pattern-forming systems*, Reports on progress in physics, 61 (1998), p. 353.
- [24] G. B. ERMENTROUT AND J. D. COWAN, *A mathematical theory of visual hallucination patterns*, Biological cybernetics, 34 (1979), pp. 137–150.

- [25] O. FAUGERAS, F. GRIMBERT, AND J.-J. SLOTINE, *Absolute stability and complete synchronization in a class of neural fields models*, SIAM Journal on applied mathematics, 69 (2008), pp. 205–250.
- [26] G. FAYE AND O. FAUGERAS, *New results for delayed neural field equations*, in Cinquième conférence plénière française de Neurosciences Computationnelles,” Neurocomp’10”, 2010.
- [27] G. FAYE, J. RANKIN, AND P. CHOSSAT, *Localized states in an unbounded neural field equation with smooth firing rate function: a multi-parameter analysis*, Journal of mathematical biology, 66 (2013), pp. 1303–1338.
- [28] J. FRASER, *A new visual illusion of direction*, British Journal of Psychology, 2 (1908), p. 307.
- [29] S. GROSSBERG, E. MINGOLLA, AND W. D. ROSS, *Visual brain and visual perception: how does the cortex do perceptual grouping?*, Trends in neurosciences, 20 (1997), pp. 106–111.
- [30] S. GROVER, W. WEN, V. VISWANATHAN, C. T. GILL, AND R. M. REINHART, *Long-lasting, dissociable improvements in working memory and long-term memory in older adults with repetitive neuromodulation*, Nature neuroscience, 25 (2022), pp. 1237–1246.
- [31] T. KATO, *Perturbation theory for linear operators*, vol. 132, Springer Science & Business Media, 2013.
- [32] C. KELLEY, *Solving Nonlinear Equations with Iterative Methods: Solvers and Examples in Julia*, SIAM, 2022.
- [33] A. KITAOKA, B. PINNA, AND G. BRELSTAFF, *Contrast polarities determine the direction of café wall tilts*, Perception, 33 (2004), pp. 11–20.
- [34] C. R. LAING, W. C. TROY, B. GUTKIN, AND G. B. ERMENTROUT, *Multiple bumps in a neuronal model of working memory*, SIAM Journal on Applied Mathematics, 63 (2002), pp. 62–97.
- [35] D. T. LILEY, P. J. CADUSCH, AND M. P. DAFILIS, *A spatially continuous mean field theory of electrocortical activity*, Network: Computation in Neural Systems, 13 (2001), p. 67.
- [36] D. MACKEY, *Visual effects of non-redundant stimulation*, Nature, 192 (1961), pp. 739–740.
- [37] D. M. MACKEY, *Moving visual images produced by regular stationary patterns*, Nature, 180 (1957), pp. 849–850.
- [38] M. NASHED AND L. B. RALL, *Nonlinear functional analysis and applications*, Differentiability and Related Properties of Nonlinear Operators: Some Aspects of the Role of Differentials in Nonlinear Functional Analysis, (1971), pp. 103–309.
- [39] R. NICKS, A. COCKS, D. AVITABILE, A. JOHNSTON, AND S. COOMBES, *Understanding sensory induced hallucinations: From neural fields to amplitude equations*, SIAM Journal on Applied Dynamical Systems, 20 (2021), pp. 1683–1714.
- [40] W. PASILLAS-LÉPINE, *Delay-induced oscillations in wilson and cowan’s model: an analysis of the subthalamo-pallidal feedback loop in healthy and parkinsonian subjects*, Biological cybernetics, 107 (2013), pp. 289–308.
- [41] A. PAZY, *Semigroups of linear operators and applications to partial differential equations*, vol. 44, Springer Science & Business Media, 2012.
- [42] M. RULE, M. STOFFREGEN, AND B. ERMENTROUT, *A model for the origin and properties of flicker-induced geometric phosphenes*, PLoS computational biology, 7 (2011), p. e1002158.
- [43] S. J. SCHIFF, *Neural control engineering: the emerging intersection between control theory and neuroscience*, MIT Press, 2011.
- [44] E. L. SCHWARTZ, *Spatial mapping in the primate sensory projection: analytic structure and relevance to perception*, Biological cybernetics, 25 (1977), pp. 181–194.
- [45] T. F. SEQUEIRA AND P. M. LIMA, *Numerical simulations of one-and two-dimensional stochastic neural field equations with delay*, Journal of Computational Neuroscience, 50 (2022), pp. 299–311.
- [46] G. M. SHEPHERD, *The synaptic organization of the brain*, Oxford university press, 2004.
- [47] C. TAMEKUE, R. CHEN, AND S. CHING, *On the control of recurrent neural networks using constant inputs*, IEEE Transactions on Automatic Control, (2025), pp. 1–16, <https://doi.org/10.1109/TAC.2025.3615934>.
- [48] C. TAMEKUE, D. PRANDI, AND Y. CHITOUR, *Reproducing sensory induced hallucinations via neural fields*, in 2022 IEEE International Conference on Image Processing (ICIP), IEEE, 2022, pp. 3326–3330.
- [49] C. TAMEKUE, D. PRANDI, AND Y. CHITOUR, *Cortical origins of mackay-type visual illusions: A case for the non-linearity*, IFAC-PapersOnLine, 56 (2023), pp. 476–481.
- [50] C. TAMEKUE, D. PRANDI, AND Y. CHITOUR, *A mathematical model of the visual mackay effect*, SIAM Journal on Applied Dynamical Systems, 23 (2024), pp. 2138–2178, <https://doi.org/10.1137/23M1616686>.
- [51] C. TAMEKUE, D. PRANDI, AND Y. CHITOUR, *Reproducibility via neural fields of visual illusions induced by localized stimuli*, Discrete and Continuous Dynamical Systems - B, 30 (2025), pp. 1441–1471.
- [52] M. TUCSNAK AND G. WEISS, *Observation and control for operator semigroups*, Springer Science & Business Media, 2009.
- [53] R. VELTZ, *Interplay between synaptic delays and propagation delays in neural field equations*, SIAM Journal on Applied Dynamical Systems, 12 (2013), pp. 1566–1612.
- [54] R. VELTZ AND O. FAUGERAS, *Local/global analysis of the stationary solutions of some neural field equations*, SIAM Journal on Applied Dynamical Systems, 9 (2010), pp. 954–998.
- [55] H. R. WILSON AND J. D. COWAN, *A mathematical theory of the functional dynamics of cortical and thalamic nervous tissue*, Kybernetik, 13 (1973), pp. 55–80.
- [56] A. ZIEPKE, S. MARTENS, AND H. ENGEL, *Control of nonlinear wave solutions to neural field equations*, SIAM Journal on Applied Dynamical Systems, 18 (2019), pp. 1015–1036.